Chemical Engineering Science 306 (2025) 121259

Contents lists available at ScienceDirect

Chemical Engineering Science

journal homepage: www.elsevier.com/locate/ces

A connectivity model for the effective thermal conductivity of a particle-filled system considering interfacial resistances

Xue Li [a], Yiqi Song [a,b], Mao Ye [a,*]

[a] National Engineering Research Center of Lower-Carbon Catalysis Technology, Dalian Institute of Chemical Physics, Chinese Academy of Sciences, Dalian 116023, China
[b] University of Chinese Academy of Sciences, Beijing, 100049, China

ARTICLE INFO

Keywords:
Effective thermal conductivity
Connectivity
Maxwell-type model
Lattice Boltzmann methods
Spatial statistics

ABSTRACT

The accurate prediction of effective thermal conductivity (ETC) of particle-filled system (PFS) is an essential but challenging topic due to the intricate structure and contact properties. Inspired by fluid flow in porous media, we propose a strategy to obtain ETC via quantifying the heat conduction pathways. Specifically, the connectivity function based on spatial statistics theory is employed to derive conduction characteristic lengths from PFS structures. By applying these characteristic lengths to Maxwell model, a generalized connectivity model is developed for discrete particles filled systems, which is validated by examining the ETCs of representative structures through inserted layer Lattice Boltzmann simulations. In comparison to traditional models, the proposed method can effectively capture the influence of anisotropic structures on ETCs in absence of specific geometry information of particles. We would stress, however, that our proposed method is particularly applicable to systems composed of irregular particles with a volume fraction lower than 25%.

1. Introduction

Particle filled systems (PFSs) are critical multiphase systems utilized in a variety of applications, including solid-void (or gas/fluid) systems in industrial packed bed reactors (van Antwerpen et al., 2010; Pietschak et al., 2020; Rodrigues et al., 2023), electrochemical devices (Fan and Wang 2011, Li, Zheng et al. 2016) and reservoirs exploration processes (Zhang et al., 2007), as well as solid–solid composite systems in material science (Ngo and Byon 2015, Rao et al., 2017). The targeted modulation of thermal conductivity of PFSs is a prevalent requirement in various applications (Pietschak et al., 2020). In this context, a comprehensive understanding of the underlying physical mechanisms and precise assessment of thermal conductivity hold significant theoretical and practical significance. Typically, effective thermal conductivity (ETC) is employed as a critical parameter for characterizing heat conduction capabilities. Extensive investigations have demonstrated that the ETC of PFS is significantly influenced by various factors, including the thermal conductivity of the particles and the matrix material, their respective volume fractions, the size, shape, orientation (Jiajun and Xiao-Su 2004, Li et al., 2016a), and arrangement(Birkholz et al., 2019) of filled particles, and the properties of interphase contact (Torquato and Rintoul 1995, Gharagozloo-Hubmann et al., 2013, Rodrigues et al., 2022). Experimental measurements of apparent ETCs are crucial (Gao et al., 2015; Zhao et al., 2020), but it is expensive to compressively consider all situations. Numerical methods provide the flexibility to treat complex structures and adjust each factor. As a result, methods for conduction (Florio 2018, Li et al., 2021b), coupled conduction–convection (Fan and Wang 2011, El Mansouri et al., 2020, Rashid et al., 2022), and conduction-radiation (Dhaidan et al., 2022, Nee and Hussein 2024) processes have been developed and successfully applied to the field such as packed beds (Chen et al., 2019, Guo et al., 2019, Rodrigues et al., 2023) and porous materials (Rong et al., 2014, Polansky et al., 2020). Based on experimental measurements and numerical results, an appropriate theoretical model that simultaneously account for all relevant factors is vital for a comprehensive understanding of the mechanisms.

Up to now, several theoretical models have been proposed (Fan and Wang 2011, Ngo et al., 2016), which can be categorized into two major approaches: effective medium approximation (EMA) and micromechanics methods (Zhai et al., 2018). The Maxwell model (Maxwell 1904), which was derived for PFSs characterized by discrete particles at low volume fractions, is the fundamental model of EMA. Subsequently, a series of studies have been conducted to extend the Maxwell model to accommodate specific structural characteristics. Bruggeman

* Corresponding author.
E-mail address: maoye@dicp.ac.cn (M. Ye).

https://doi.org/10.1016/j.ces.2025.121259
Received 12 November 2024; Received in revised form 27 December 2024; Accepted 21 January 2025
Available online 25 January 2025

(Bruggeman 1935) and Landauer (Landauer 2004) formulated an implicit expression to account for the influence of each inclusion on the local temperature field, thereby contributing to the development of the effective medium theory (EMT) model, which is applicable to PFSs with complex structures and moderate particle volume fractions. A comparable approach was proposed based on the reciprocity theorem for uniformly mixed systems (del Río et al., 1998). Additionally, the effects of particle shape (Fricke 1953, Hamilton and Crosser 1962), orientation (Nan et al., 1997), size and thermal contact resistance (TCR) (Benveniste 1987, Hasselman and Johnson 1987, Xu et al., 2016b) have also been investigated. However, these models are constrained to particles with regular geometry.

The micromechanics methods include the variational principle and the mean field approximation. Hashin and Shtrikman (Hashin and Shtrikman 1962) employed variational theorems to establish the bounds of effective magnetic permeability, as well as electrical and thermal conductivity, which show the same form as the Maxwell model. Mori and Tanaka related the averaged stresses and strain in inclusion to those of matrix (Mori and Tanaka 1973). Benveniste further developed this method by using Eshelby's Equivalent inclusion theory to account for imperfect surfaces (Benveniste 1987). Meanwhile, several semi-empirical models that analogize thermal conduction to electrical conduction have been proposed. In these methods the particles and the matrix are regarded as elements forming a circuit network. Consequently, the challenge lies in assessing the conductivity of the network. In limiting cases, the two components can be disaggregated into layers that are either parallel or perpendicular to the direction of heat flux, thereby formulating the parallel and series models, which service as the upper and lower bound of the microscopic component models (Wiener 1912, Deissler, 1958). Agari and Uno (Agari and Uno 1986) introduced several parameters to reconstruct the parallel/series model to present the variations in conductive chains. Hsu et al. (Hsu et al., 1995) proposed a lumped-parameter model for periodically arranged particles in contact with each other, which is particularly applicable to packed beds (van Antwerpen et al., 2010). The fractal theory has also been employed to characterize branched networks (Xu et al., 2006, Qin and Yin 2023). However, these latter models incorporate semi-empirical parameters that are difficult to ascertain. Various efforts have been made to acquire mesoscopic ensembles containing microscopic states (Lipton 1997, Xu et al., 2016a), nevertheless, the integration and variation processes remain complex. By primarily focusing on the connecting characteristics, the network models considering local microstructures (Liang and Li 2014, Wang and Li 2017, Birkholz et al., 2019) can yield reasonable results with significantly reduced evaluation complexity, but they are heavily dependent on the geometry of the study field. There exists a notable absence of objective and robust structure parameters.

Although the aforementioned theoretical models have demonstrated effectiveness for various scenarios, the selection of appropriate models and the specific modification of corresponding parameters are indispensable for each practical application (Carson et al., 2005). A common selection principle can be referred in Fig. 1 (Carson et al., 2005), which shows the curves of some fundamental theoretical models (k_e/k_m) with $k_p/k_m = 100$ where k represents the thermal conductivity, and subscripts e, p, m denote the entire system, the particle (characterized by high thermal conductivity), and the matrix, respectively. The significant disparities observed in the prediction curves underscore the importance of a quantitative and universal description of microstructures. Intuitively, in a particle-filled system, heat, akin to fluid in a porous medium, preferentially travels along pathways with higher conductivity. Consequently, characterization methods employed in porous media flow such as the spatial statistics methodology may be advantageous for the study of thermal conduction.

Spatial statistics is a mature methodology (Journel 1993, Mariethoz and Caers 2014) that provides several quantitative tools for the characterization of complex geometric structures based on Monte Carlo stochastic theory and statistics theory. These spatial statistical techniques have been widely applied for the accurate reconstruction of porous media and the characterization of their flow and transport properties (Klise et al., 2009). Researches have indicated that the flow and transport properties within porous structures are closely associated with realistic connectivity patterns (Journel 1993, Klise et al., 2009, Li et al., 2016b), which are likely to be critical parameters in heat conduction. Connectivity has been exhaustively studies and its characteristic length can be effectively assessed by experts or numerically calculated with a connectivity function (Journel 1993, Mariethoz and Caers 2014). In systems filled with discrete particles, the connectivity characteristic lengths of the particle phase directly reflect the geometric features of the particle–matrix structures, regardless of pre-processing (e.g., regularization approximations of irregular particles) and the specific attributes of individual particles (e.g., shape, size, orientation, and arrangement). Consequently, the connectivity characteristic lengths are more appropriate than the case-independent particle geometry parameters to formulate a unified theoretical model. Accordingly, this study develops a connectivity model based on the Maxwell model for PFSs with non-contacting particles at low volume fractions. The proposed connectivity model unifies various Maxwell-type variants for different fillers, improving prediction accuracy and expanding applicable scenarios.

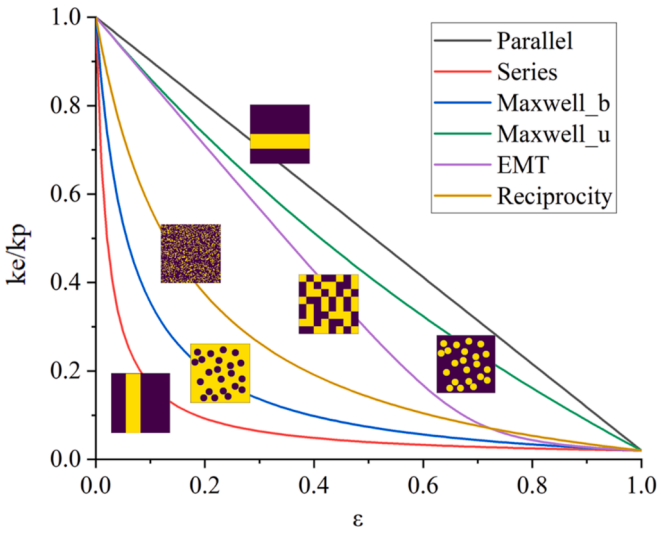

Fig. 1. Schematic representations of the structure assumed by each theoretical model.

In the following sections, the conception and implementation of the connectivity function are presented. Subsequently, the connectivity-based model is proposed and validated using data reported in the literature in section 2. Section 3 introduces an insert layer Lattice Boltzmann method (LBM) to investigate the detailed heat conduction processes, taking into account thermal contact resistances (TCRs). The simulated ETCs will be used for comparison in subsequent analyses. In section 4, the proposed model is utilized to evaluate the ETCs of various structures filled with non-uniform and irregular particles, which are commonly encountered in practical applications. The evaluated results are compared with simulation results and those of previous models. The influence of particle size, shape, orientation, and arrangement is discussed, and the advantages of the proposed method on the arbitrary shaped particles are presented. Finally, conclusions and drawn, and implications for futures are outlined.

2. Model description

In this section, the spatial statistical tool known as the connectivity function is introduced and utilized to analyze the typical structures assumed by each theoretical model. Subsequently, the obtained

connectivity characteristic lengths are utilized to formulate a Maxwell-type model following previous analytical models. The proposed model is validated on PFSs with typical shaped fillers reported in the literature.

2.1. Spatial statistics theory and connectivity function

The spatial statistics theory studies spatial variables. Consider a particle-filled geometric structure consisting of two phases (particle and matrix) as a spatial field with categorical variables $\{s(\boldsymbol{x}_1), s(\boldsymbol{x}_2), \cdots\}$ taking value of s_i at locations $\boldsymbol{x}_1, \boldsymbol{x}_2, \cdots$. In this manuscript, the subscript i denotes p for particle phase and m for matrix phase.

In a Cartesian grid, if $n+1$ adjacent spatial variables along a specified direction $\boldsymbol{d}$ have the same value $s(\boldsymbol{x} \leftrightarrow \boldsymbol{x}+n\boldsymbol{d}) = s_i$, they are connected at the distance vector of $n\boldsymbol{d}$. The connectivity function utilizes the conditional probability function to describe how one category is connected. By searching all spatial variable sets $\{s(\boldsymbol{x}) \leftrightarrow s(\boldsymbol{x}+n\boldsymbol{d})\}$, the connectivity function depending on distance vector $n\boldsymbol{d}$ is calculated by:

$$C_i(n\boldsymbol{d}) = Prob\{s(\boldsymbol{x} \leftrightarrow \boldsymbol{x}+n\boldsymbol{d}) = s_i | s(\boldsymbol{x}) = s_i, s(\boldsymbol{x}+n\boldsymbol{d}) = s_i\} \quad (1)$$

where n is a positive integer. For further details, one can refer to some handbook (Goovaerts 1998) and the associated application works (Li, Tan et al. 2021). A simple example is presented in Fig. 2(a), which depicts a 4×5 structure consisted of "white" and "gray" two phases. Traversing the entire domain with the condition $\{s(\boldsymbol{x}) = "gray", s(\boldsymbol{x}+2\boldsymbol{d}) = "gray"\}$, there are two sets could be found, of which only the set on location $\boldsymbol{x}1$ satisfies $\{s(\boldsymbol{x} \leftrightarrow \boldsymbol{x}+2\boldsymbol{d}) = "gray"\}$. Then the connectivity on $2\boldsymbol{d}$ is calculated as: $C_{gray}(2\boldsymbol{d}) = 1/2$. As n ranges from 1 to encompass the length of the study field, the distribution curve of connectivity as a function of distance ($n\boldsymbol{d}$) can be drawn, and the characteristic length of connectivity can be estimated. The essential aspects are elaborated in Fig. 2 (b)-(d).

Fig. 2(b) Is a typical pfs expressed by a 500×500 pixels digital graph. In order to study the horizontal thermal conductivity, it is essential to focus on the heat flux in the horizontal direction, necessitating the characteristic lengths of connectivity both along and perpendicular to this direction. This analysis aims to elucidate anisotropic heterogeneity of PFSs. Since the matrix is a continuous phase, its connectivity function maintains a constant value of 1. In contrast, for the particle phase, connectivity decreases gradually from 1 as distance increases, ultimately stabilizing at the value of 0. The trends observed in the connectivity distribution curves reflect the spatial structure features, including the shape, size, and arrangement of the particles. The length at which the connectivity distribution function first reaches the stable value of 0 can be defined as the connectivity characteristic length. However, this definition presents two significant issues. Firstly, the results may exhibit bias. In instances if filled particles within in a PFS are uniform, this length is the characteristic length of the particle (e.g., the diameter of a circular particle). Conversely, when the filled particles differ, as depicted in Fig. 2(b), the length is the maximum occupied distance of all filled particles along the corresponding direction. Thus, the presence of one or several anomalous particles may yield unreasonable results. Secondly, this definition ignores detailed spatial structure features. Numerous studies have demonstrated that different particle arrangements within PFSs give rise to diverse transport characteristics. When assessing the overall regional transport properties through local sampling areas, different sample regions will yield different outcomes. The uncertain deviation between sample results and the true value (Caers, 2011) poses a challenge in the study of randomly filled PFSs. To mitigate these issues, spatial statistics recommend fitting the connectivity distribution curve to eliminate outliers associated with abnormal particles and to incorporate the detailed spatial features represented by the distribution curve (Goovaerts 1998, Caers 2011). Fig. 2 (c) and (d) displayed the calculated connectivity distribution and the fitted curves along and perpendicular to the heat flux direction, respectively. The original calculated and locally Gaussian fitted characteristic lengths L are indicated by dashed lines. The subscripts // and $\perp$ denote the directions along and perpendicular to the heat flux direction, while the superscript "o" indicates the original calculated value.

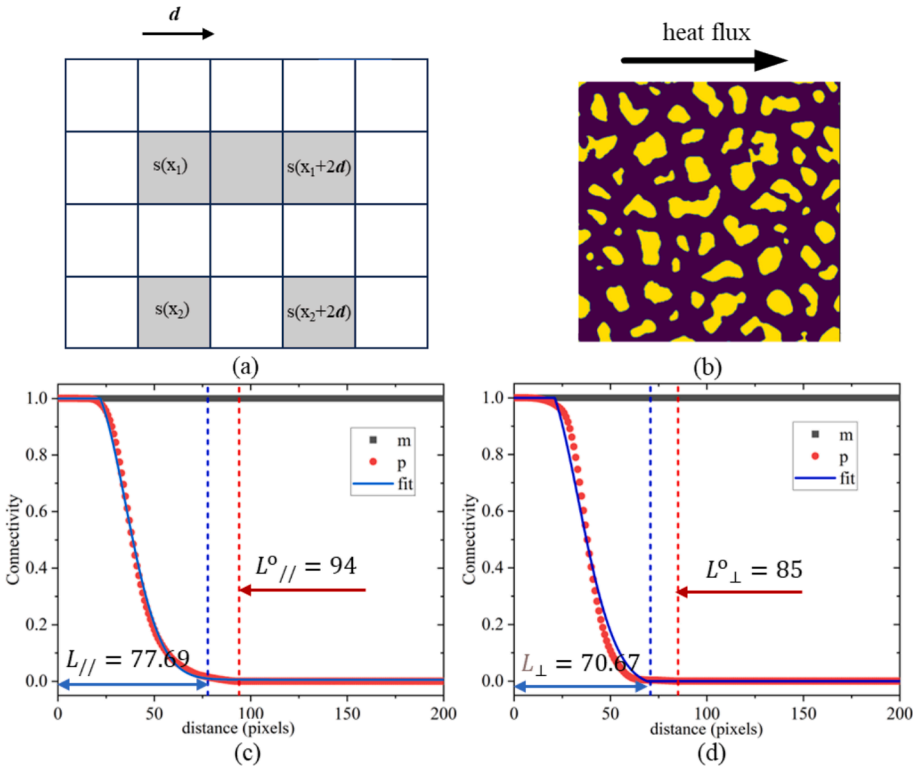

Fig. 2. (a)Illustration of the calculation of connectivity; (b) a typical PFS structure and heat flux; connectivity distribution functions and the evaluated connectivity characteristic length (c) along and (d) perpendicular to the direction of heat flux.

In this instance, the originally calculated zero-value points are 94 and 85 pixels, whereas the Gaussian fitted value for L are 77.69 and 70.67 pixels at a 99 % confidence interval for each direction. By reconciling the effects of individual particles and incorporating spatial distribution information, the fitted results demonstrate greater statistical significance than the original calculated data and exhibit enhanced consistency with the presented structure.

2.2. Connectivity function for typical PFS structures

By applying the connectivity distribution function, the typical structures assumed by each theoretical model shown in Fig. 1 can be clearly distinguished as shown in Fig. 3.

Fig. 3 focus on heat conduction in horizontal direction. The parallel model assumes the two components are layers arranged in parallel to the heat flux direction, as illustrated in Fig. 3(a)). Consequently, the corresponding connectivity distribution function is fixed at a value of 1 for both phases, as shown in Fig. 3(f). In contrast, the serial structure shown in Fig. 3(b) features a connectivity function that delineates the width of the discrete layer, as shown in Fig. 3(g). Given that the serial structure is a ninety-degree rotation of the parallel structure, the connectivity function parallel to heat flux direction in one configuration equals to the connectivity function perpendicular to the heat flux direction in the other configuration. Fig. 3(c) illustrates a structure composed of discretely distributed circular particles, as assumed by the classical Maxwell model. The corresponding connectivity distribution curve shown in Fig. 3(h) exhibits similarities to the results of the example shown in Fig. 2. The EMT model is developed for structures in which particles close or connecting to each other as shown in Fig. 3(d). The corresponding connectivity function begins with a sill of 1 representing the basic length, and then gradually decreases to 0, as shown in Fig. 3(i). A similar descending trend without the sill is observed in Fig. 3(j) for the homogeneous mixing structure assumed by reciprocity model.

It indicates that the connectivity function can effectively distinguish the geometric structures assumed by fundamental theoretical models. Therefore, incorporating connectivity information in the theoretical model for ETC evaluation has the potential to include more detailed structure information. The attempt to incorporate the connectivity characteristic lengths in Maxwell-type model is presented in the next subsection.

2.3. Connectivity-based model for ETC

In this section, a connectivity-based model is developed based on Maxwell theoretical analysis since it is the most theoretically robust and frequently employed framework for particle-filled systems. Several variants of this model have been developed to address diverse structural characteristics, as illustrated in Table 1.

In Table 1, Ψ denotes the sphericity which is defined as the ratio of the surface area of a sphere with the same volume as the particle considered to the surface area of the particle, D takes the value of 3 for three-dimensional (3D) cases and 2 for two-dimensional (2D) cases, R_c denotes the interfacial thermal barrier resistance or TCRs, r denotes particle radius, $\langle cos^2\theta \rangle$ is the average particle orientation, L_{11} and $\beta_{//}$ are the shape parameters along heat flux direction, while L_{33} and $\beta_{\perp}$ are the shape parameters orthogonal to heat flux direction. Eq.(5) provides a calculation for the Kapitza radius r_k, which is widely used to represent the effective length of TCRs within PFSs. This definition is also utilized in the present study.

Despite these variants aiming to the modification of derivation and incorporating the effects of the particle–substrate geometry, the constraints imposed by the over-idealized assumptions persists. For example, Nan's model considers the influence of the orientation of non-spherical particles and showed good results in cases involving typical shaped particles. Additionally, the flatness ratio model (Chu et al., 2013) deriving from Nan's model has been successfully applied to the graphene nanotubes composites where the orientation is a key parameter. However, the parameters related to shape and orientation are challenging to obtain and are limited to regular shaped particles.

Fortunately, this structure information is inherently embedded within the connectivity distribution curves. Consequently, following the framework established in Eq. (7), a connectivity model is constructed as:

$$k_e = k_m \frac{(f-1)k_m + \left[1+(f-1)R_c^*\right]k_p - (f-1)\left[k_m - \left(1-R_c^*\right)k_p\right]}{(f-1)k_m + \left[1+(f-1)R_c^*\right]k_p + \left[k_m - \left(1-R_c^*\right)k_p\right]} \quad (13)$$

with the dimensionless contact resistance R_c^* and the morphological parameter f defined by the connectivity characteristic length $L_{//}$ and $L_{\perp}$ as:

$$R_c^* = 2r_k/L_{//} \quad (14)$$

$$f = D/\Psi_s \quad (15)$$

$$\Psi_s = \sqrt{\Psi L_{\perp}/L_{//}} \quad (16)$$

The connectivity characteristic length along heat flux direction $L_{//}$ rather than the equivalent particle radius r in Eq.(6) is utilized to measure the influence of thermal resistance. This treatment is analogous to considering the axis length along heat flux direction as the equivalent diameter, which is suggested by several researchers (Nan et al., 2000, Ke and Duan 2019). The morphological parameter f incorporates the aspect ratio of the connectivity length ($L_{\perp}/L_{//}$) as well as the sphericity of the particle. Specifically, sphericity reflects the impact of contact area at a certain volume fraction, while the aspect ratio represents the combined effects of the enhancement with an increasing connectivity along heat flux and the obstruction with an increasing connectivity perpendicular to the heat flux as suggested by Nan's model. Since the connectivity function contains spatial distribution information based on spatial statistics theory, the proposed method directly conveys orientation distribution information of non-spherical particles, eliminating the need for detailed information about individual particles.

2.4. Tests for structures with typical shaped fillers

To verify the feasibility of the proposed model, the ETCs of structures filled with some typical shaped fillers are evaluated using the proposed model and compared with the reported data which has been experimental and numerical verified in literatures (Zhang et al., 2013, Rao et al., 2017;). In these investigations, a single particle was positioned at the center of the two-dimensional study field, thus the connectivity related parameters along the major (vertical) and minor (horizontal) axes denoted as Ψ_{s1} and Ψ_{s2} can be calculated by using the particle length as the connectivity characteristic length as mentioned in section 2.1. Table 2 lists the shape of these particles and the corresponding connectivity parameters utilized in the proposed model.

The effects of particle shape and orientation on ETCs have been investigated by Zhang *et al.* (Zhang et al., 2013) through both numerical and experimental methods. One set of results was selected at the filler volume fraction of 10 %, where thermal conductivity of filler and matrix is 209 W/m·K and 0.29 W/m·K, respectively, yielding a ratio of 720.7. The reference data and the evaluation results obtained using the Maxwell model, the Fricke-Hamilton-Crosser (FHC) model expressed with Eq.(4), and the proposed model are compared in Fig. 4. It shows that particle shape significantly influences ETCs, and the evaluation results from the proposed model are closest to the reference data for most cases. The FHC model using sphericity to reflect the influence of filler shape and obtains good results when the characteristic length of the particle along both axes is similar, such as square and triangle. In addition to sphericity, the proposed model incorporates the aspect ratio of the connectivity characteristic lengths along the major and minor

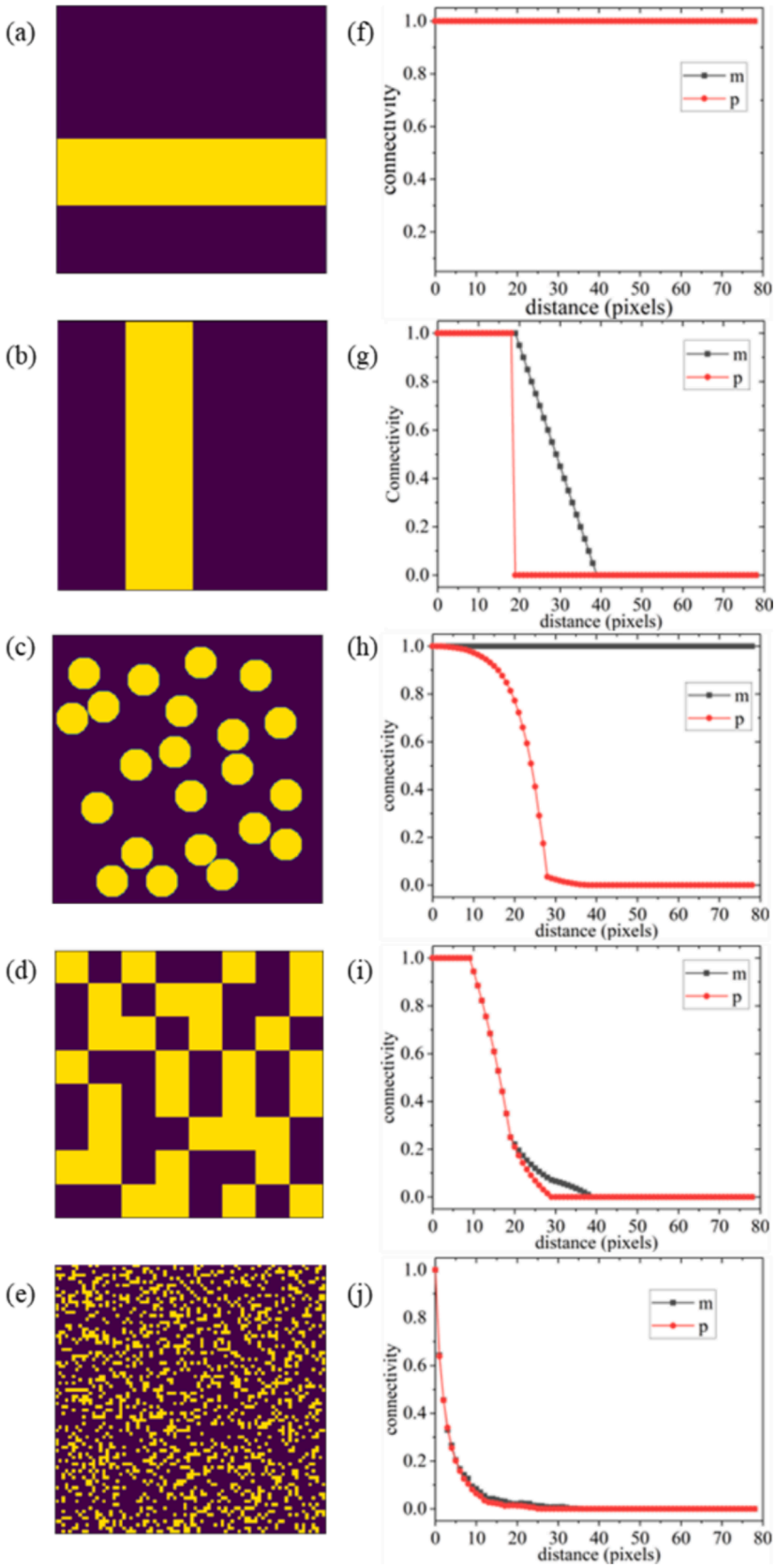

Fig. 3. Connectivity function for the typical structures assumed by each theoretical model. (a)-(e) typical structures where the yellow phase has a high thermal conductivity presented by *p* and the blue phase has a low thermal conductivity presented by *m*; (f)-(j) the corresponding connectivity distribution curve for each phase along horizonal direction.

Table 1
The variants of Maxwell-type ETC models.

Model	Formular	Description
Maxwell model (Maxwell 1904)	$k_e = k_m \frac{2k_m + k_p - 2(k_m - k_p)\phi}{2k_m + k_p + (k_m - k_p)\phi}$ (2)	dispersed spherical particles, low volume fractions
	ϕ denotes the volume fraction of particles	
Fricke(Fricke 1953) and Hamilton and Crosser(Hamilton and Crosser 1962) model	$k_e = k_m \frac{(\Lambda-1)k_m + k_p - (\Lambda-1)(k_m - k_p)\phi}{(\Lambda-1)k_m + k_p + (k_m - k_p)\phi}$ (3)	Consider particle shapes
	$\Lambda = D/\Psi$ denotes the shape factor	
Hasselman and John (Hasselman and Johnson 1987) and Benvensite (Benveniste 1987) model	$k_e = k_m \frac{2k_m + (1+2r_c)k_p - 2[k_m - (1-r_c)k_p]\phi}{2k_m + (1+2r_c)k_p + [k_m - (1-r_c)k_p]\phi}$ (4)	Consider TCRs
	$r_k = R_c k_m$ (5)	
	$r_c = r_k / r$ (6)	
	$k_e = k_m \frac{(\Lambda-1)k_m + [1+(\Lambda-1)r_c]k_p - (\Lambda-1)[k_m - (1-r_c)k_p]\phi}{(\Lambda-1)k_m + [1+(\Lambda-1)r_c]k_p + [k_m - (1-r_c)k_p]\phi}$ (7)	Consider both particle shapes and TCRs
Nan et al.(Nan, Birringer et al. 1997, Nan, Li et al. 2000) model Nan et al., 1997; Nan et al., 2000	$\frac{k_\perp}{k_m} = \frac{2 + \left[\beta_\perp(1-L_{11})(1+\langle cos^2\theta\rangle) + 2\beta_{//}L_{11}(1-\langle cos^2\theta\rangle)\right]\phi}{2 - \left[\beta_\perp L_{11}(1+\langle cos^2\theta\rangle) + \beta_{//}L_{33}(1-\langle cos^2\theta\rangle)\right]\phi}$ (8.a)	Consider orientation of non-spherical particles
	$\frac{k_{//}}{k_m} = \frac{1 + \left[\beta_\perp(1-L_{11})(1-\langle cos^2\theta\rangle) + 2\beta_{//}L_{11}\langle cos^2\theta\rangle\right]\phi}{1 - \left[\beta_\perp L_{11}(1-\langle cos^2\theta\rangle) + \beta_{//}L_{33}\langle cos^2\theta\rangle\right]\phi}$ (8.b)	
EMT model (Landauer 2004)	$(1-\phi)\frac{k_m - k_e}{k_m + 2k_e} + \phi\frac{k_p - k_e}{k_p + 2k_e} = 0$ (9)	Considering the influence of particles on the matrix
Bruggeman model (Bruggeman 1935)	$1-\phi = \frac{k_p - k_e}{k_p - k_m}\left(\frac{k_m}{k_e}\right)^{1/3}$ (10)	Integral form of EMT model
Every model (Every et al., 1992)	$(1-\phi)^3 = \left(\frac{(1-r_c)k_p - k_e}{(1-r_c)k_p - k_m}\right)^{3/(1-r_c)}\left(\frac{k_m}{k_e}\right)^{(1+2r_c)/(1-r_c)}$ (11)	consider TCRs
Wang and Yi model (Jiajun and Xiao-Su 2004)	$(1-\phi)^\Lambda = \left(\frac{(1-r_c)k_p - k_e}{(1-r_c)k_p - k_m}\right)^{\Lambda/(1-r_c)}\left(\frac{k_m}{k_e}\right)^{(1-r_c+\Lambda r_c)/(1-r_c)}$ (12)	Consider TCRs and particle shape

axes, thereby further illustrating the change trend of ETCs along different directions.

Note that, based on the spatial statistical theory, the connectivity distribution function is more appropriate for describing random distribution systems. Consequently, the comparison with single particle systems may be regarded as a qualitative validation of the proposed model. More detailed and quantitative investigations will be presented in the subsequent sections.

3. Numerical methods

In order to demonstrate the effectiveness of the proposed model on a variety of structures, several digital PFS structures are numerically generated and numerical simulation methods are implemented to obtain the detailed heat transfer processes. Many numerical methods including the finite volume model (Vieira and Marques 2019), the finite element method (Tian et al., 2019), and Lattice Boltzmann method have been developed. In this context, the inserted layer Lattice Boltzmann Method proposed in our previous work (Li et al., 2021a) is utilized.

3.1. Thermal LBM model

According to Fourier's law, the heat conduction in multi-phase systems in governed by:

$$\frac{\partial T_i}{\partial t} = \frac{k_i}{(\rho c_P)_i}\nabla^2 T_i + Q_i \tag{17}$$

where T is the temperature, ρc_P is the volumetric heat capacity, Q is the source term, and the subscript i represents the matrix and particle components. Then the ETC can be calculated as:

$$-k_e = Lq/\Delta T \tag{18}$$

where q is the steady flux through the computation field with a thickness of L and temperature difference ΔT. In the LBM, the distribution function h is utilized to recover Eq.(16) with a collision and a streaming step as:

$$\widehat{h}_\alpha(\boldsymbol{x}, t) = h_\alpha(\boldsymbol{x}, t) - \Omega(h - h^{eq}) + w_\alpha Q\delta t \tag{19}$$

$$h_\alpha(\boldsymbol{x} + \boldsymbol{e}_\alpha\delta t, t + \delta t) = \widehat{h}_\alpha(\boldsymbol{x}, t) \tag{20}$$

where $\widehat{h}$ is the post-collision state, w is the weight for the α th distribution directions $\boldsymbol{e}$

If two components perfectly contact with each other, continuous boundary conditions are satisfied for both temperature and heat flux. The conjugated interface can be treated as:

$$h_{\overline{\alpha}}(\boldsymbol{x}, t + \delta t) = \frac{(\rho c_P)_{\boldsymbol{x}} - (\rho c_P)_{\boldsymbol{x}+\boldsymbol{e}_\alpha}}{(\rho c_P)_{\boldsymbol{x}} + (\rho c_P)_{\boldsymbol{x}+\boldsymbol{e}_\alpha}}\widehat{h}_\alpha(\boldsymbol{x}, t) + \frac{2(\rho c_P)_{\boldsymbol{x}+\boldsymbol{e}_\alpha}}{(\rho c_P)_{\boldsymbol{x}} + (\rho c_P)_{\boldsymbol{x}+\boldsymbol{e}_\alpha}}\widehat{h}_{\overline{\alpha}}(\boldsymbol{x} + \boldsymbol{e}_\alpha\delta t, t) \tag{21}$$

where the subscript $\overline{\alpha}$ denotes the opposite direction of the α th distribution directions.

When TCRs presents, a temperature discontinuous and flux continuous boundary condition is described according to the Kapitza model (Kapitza 1941). The treatment of discontinuous boundary conditions is difficult in numerical simulations, which may increase numerical instability or reduce computational efficiency. In our previous work, by considering the interfacial resistance as a known variable, an inserted layer strategy was proposed to convert discontinuous boundaries to continuous ones by inserting a virtual point as illustrated in Fig. 5.

In this method, the inserted TCR nodes at imperfect interface satisfies the continuous flux boundary as:

$$k_1 A_1 \frac{T_1 - T_{C1}}{L_1} = A_C \frac{T_{C1} - T_{C2}}{Rc} = k_2 A_2 \frac{T_{C2} - T_2}{L_2} \tag{22}$$

At the same time, the discontinuous temperature boundary conditions between the two objects ($T_{C1} \neq T_{C2}$) are concerted into the continuous temperature boundary conditions between the studied components and the inserted TCR nodes. Therefore, the interface treatment can be reformulated based on Eq.(21). The boundary treatment for inserted TCR node at $\boldsymbol{x_c}$ and the relative adjacent node $\boldsymbol{x} = \boldsymbol{x_c} + \boldsymbol{e}_\alpha\delta t$ at $\boldsymbol{e}_\alpha$ direction is derived as:

Table 2
Comparison of particle parameters and connectivity related parameters on typical shaped fillers (Zhang et al., 2013, Rao et al., 2017).

Filler name	Shape	Ψ	L_{major}	L_{minor}	Ψ_{s1}	Ψ_{s2}
Circular		1	1	1	1	1
Square		0.8862	0.8862	0.8862	0.9414	0.9414
Equilateral triangular		0.7776	1.1663	1.3468	0.8206	0.9476
Rhombic	 $\beta = 60$ $\beta = 60^{\circ}$	0.8247	1.6495	0.9523	0.6900	1.1952
Elliptical	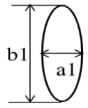 $\frac{a_1}{b_1} = \frac{1}{3}$ $\frac{a_1}{b_1} = \frac{1}{3}$	0.7619	1.7321	0.5774	0.5040	1.5118
Rectangular	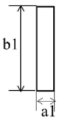 $\frac{a_1}{b_1} = \frac{1}{5}$ $\frac{a_1}{b_1} = \frac{1}{5}$	0.6606	1.9817	0.3963	0.3635	1.8175
T shape	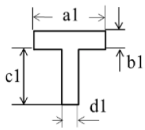 $a_1 = \frac{5}{4}c_1 = 5b_1 = 5d_1$ $a_1 = \frac{5}{4}c_1 = 5b_1 = 5d_1$	0.5317	1.4770	1.4770	0.7292	0.7292
I shape	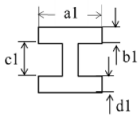 $a_1 = \frac{5}{3}c_1 = 5b_1 = 5d_1$ $a_1 = \frac{5}{3}c_1 = 5b_1 = 5d_1$	0.4565	1.2290	1.2290	0.6756	0.6756

$$h_{\bar{\alpha}}(\boldsymbol{x}_c, t+\delta t) = \frac{1-(\rho c_P)_{\boldsymbol{x}}}{1+(\rho c_P)_{\boldsymbol{x}}}\widehat{h}_{\alpha}(\boldsymbol{x}_c, t) + \frac{2(\rho c_P)_{\boldsymbol{x}}}{1+(\rho c_P)_{\boldsymbol{x}}}\widehat{h}_{\bar{\alpha}}(\boldsymbol{x}, t) \tag{23.1}$$

$$h_{\alpha}(\boldsymbol{x}, t+\delta t) = \frac{(\rho c_P)_{\boldsymbol{x}}-1}{(\rho c_P)_{\boldsymbol{x}}+1}\widehat{h}_{\alpha}(\boldsymbol{x}, t) + \frac{2}{(\rho c_P)_{\boldsymbol{x}}+1}\widehat{h}_{\bar{\alpha}}(\boldsymbol{x}_c, t) \tag{23.2}$$

where the volumetric heat capacity of the virtual TCR nodes is settled to 1 to keep consistence with the definition of resistance *Rc*. For more details one can refer to the algorithm work (Li et al., 2021a).

The present LBM mothed has been exhaustively tested and shows good numerical stability and high computational efficiency. The simulation results on typical structures including parallel, series and circular fillers provide a good agreement with analytical solutions and results from commonly used numerical models. In this paper, this model is utilized to calculated the ETCs of several typical PFS structures in engineering applications as the baseline for theoretical models.

3.2. Numerical parameters

In the present study, a two-dimensional (2D) study field of 250 × 250 lattice in LBM unit is considered. The horizontal direction is defined as the x-axis, while the vertical direction is defined as the y-axis. Insulated boundaries are settled on the top and bottom, a fixed temperature of 20 °C is maintained at the right boundary, and a fixed flux of 8.0×10^{-3} in LBM units is applied on the left boundary. It is important to note that the boundary conditions do not impact the evaluation results of ETCs, and such boundary conditions are frequently employed in numerical simulations since it is similar to experimental conditions utilized in the heat flow method (Zhang et al., 2013). Furthermore, the volumetric heat capacity has no significant effect on the results of ETCs, thus a value of 1

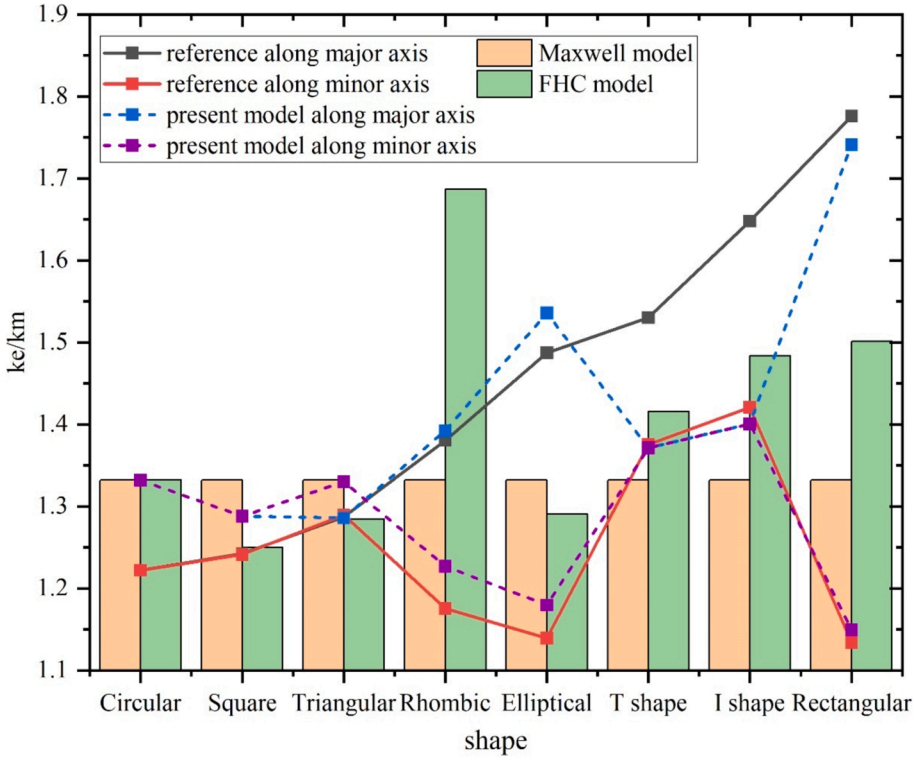

Fig. 4. ETCs along the major and minor axes for typical shaped fillers. The thermal conduct ratio of the particles and matrix is 720.7, and the volume fraction of the filler is 10%.

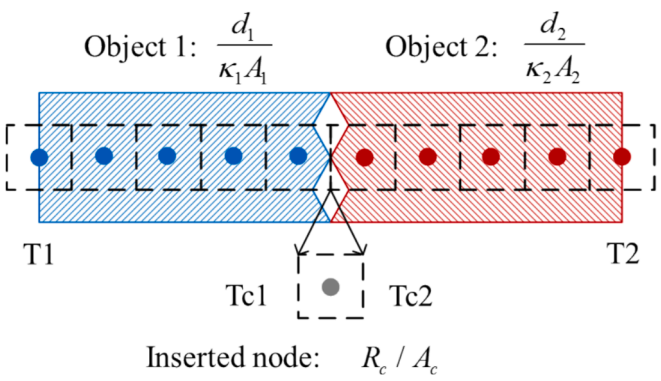

Fig. 5. The insert layer strategy for Kapitza contact resistance (Li, Gao et al. 2021).

is assigned to both components to simplify the calculations.

In general, the Maxwell model is recommended for systems with a particle volume fraction below 10 %, as evaluation errors tend to increase with higher particle volume fractions. However, several studies have indicated that the predictions mode by the Maxwell model remain acceptable to a certain extent at a slightly elevated volume fraction. Given that the present study examines spatial statistical connectivity, it is essential to include enough particles to ensure statistical validity. When addressing smaller volume fractions, a larger computational domain is required, which significantly increase the computational resources needed. Consequently, a particle volume fraction of approximately 25 % is considered as a reasonable compromise (Ke and Duan 2019). An example of a PFS filled with circular particles is presented in Fig. 6. The three structures denoted as C1, C2, and C3, contain circular fillers with different radii of 15, 26 and 34 lattices (in LBM units and the same in the following of the work) within the simulation grid, all of which have successfully passed the grid independence tests. Due to the lattice resolution, the actual particle volume fractions for the three structures is 24.5 %, 23.6 %, and 23.4 %, respectively. In the study of TCR's impact on ETC, the Kapitza radius r_k is crucial. It is generally accepted that when r_k is equal to the particle radius, the overall ETC is equal to k_m, while when it is larger than the particle radius, the ETC will be smaller than k_m, and vice versa (Benveniste 1987). Therefore, for the three particle sizes mentioned above, this study investigates the situation at Kapitza radii of 0, 7.5, 15, 26, 39 and 45 lattice. In this section, the conductivity ratio between the particle and the matrix is settled at 100.

Fig. 6 presents a comparison of the simulation results with and without considering TCRs. In the absence of TCRs, a smaller temperature difference ΔT between the two boundaries is observed across all three structures, indicating that TCRs prevent heat conduction processes. The simulated ETCs are displayed in Fig. 7. When TCRs are not taken into account only minor variations are observed for different particle sizes, which may come from the small differences in the particle volume fractions of the three structures. Whereas the differences increase progressively with the increasing of TCRs. This phenomenon matches well with existing experimental observations (Gao et al., 2015) and numerical simulations (Ke and Duan 2019). These results will be used as the baseline data for the studies in the subsequent section.

4. Results and discussion

In this section, the ETCs of three typical 2D PFS structures and a 3D PFS structures are exhaustive investigated using LBM simulations and the proposed model. The influence of size distribution, orientation, and shape of the fillers on heat transfer performance is analyzed. This section describes the relationship between these factors and the proposed connectivity-related parameters in detail, then further, discusses the efficacy of the proposed method in scenarios where specific information regarding the fillers in unavailable.

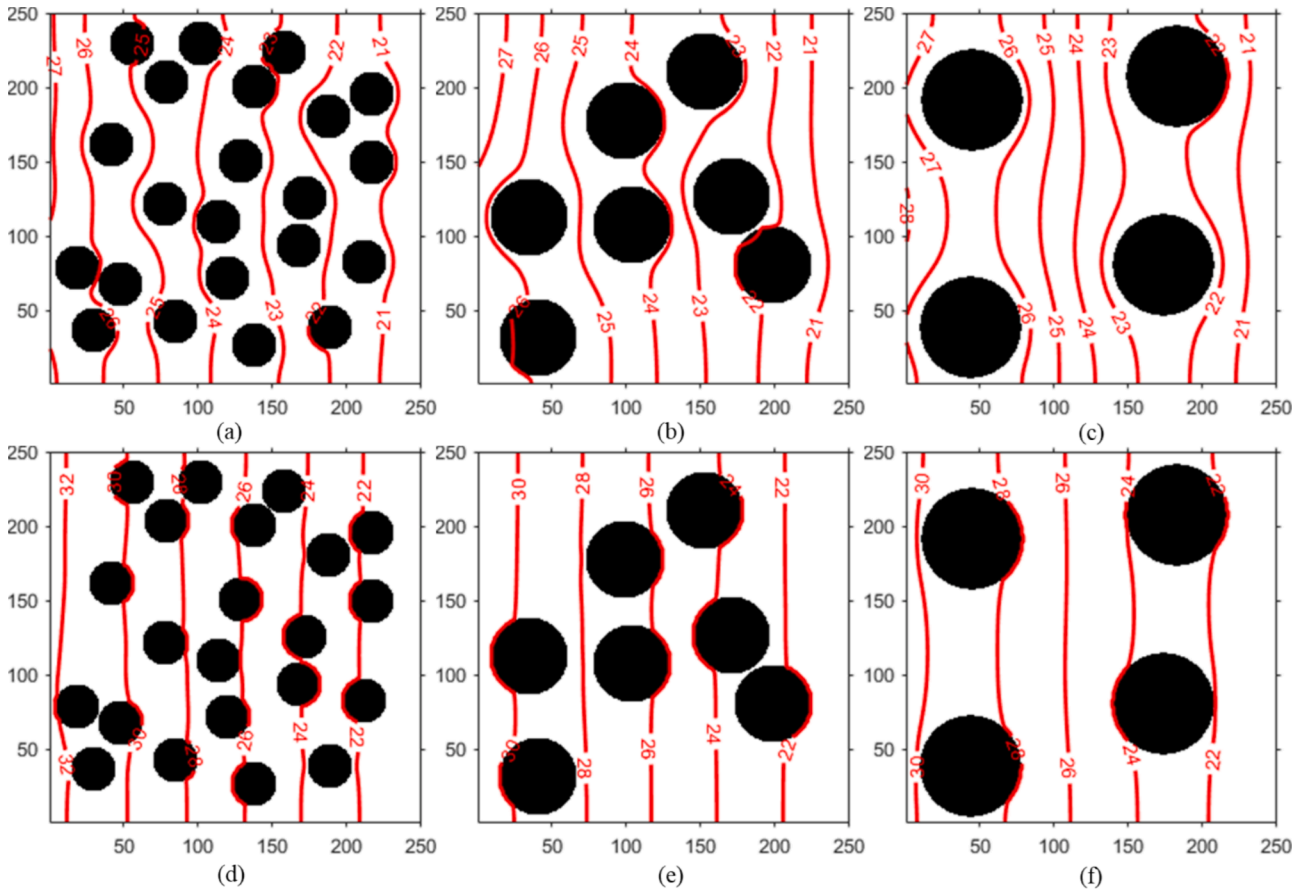

Fig. 6. Structures filled with circular particles of varying sizes and the corresponding simulations: (a)-(c) $r_k = 0$; (d)-(f) $r_k = 26$ (lattice).

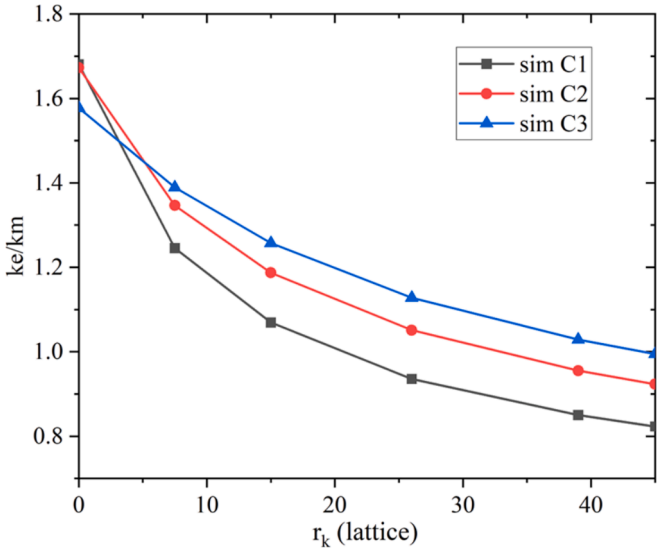

Fig. 7. Simulated ETCs for each structure under $r_k = 0, 7.5, 15, 26, 39,$ *and*45 lattice.

4.1. PFS structures with fillers of different size distributions

In practical applications, particles are often non-uniform with respect to their sizes. This section examines the influence of varying size distributions of fillers on ETCs. Utilizing structure C1 as the reference, two structures with the same mean diameter as C1 but different ranges of variation are generated. The particle radii are modeled according to a normal distribution, with the maximum range of 3 lattice and 5 lattice for the two structures, denoted as CR1 and CR2, respectively are generated. To ensure the average radius remains consistent with the diameter of C1 for comparison purposes, a post-processing step is operated to adjust the size of some particles in CR1 and CR2. The corresponding radius distributions are shown in Fig. 8.

Two simulation results for these structures and the connectivity functions for each structure are displayed in Fig. 9.

In the case of isotropic distributed discrete particle structures, the connectivity functions in the two orthogonal directions exhibit a high degree of similarity. Fig. 9(e) displays the connectivity distribution functions along the heat flux direction (x-axis). Since the particle sizes in CR1 and CR2 follow a normal distribution, the connectivity characteristic length is approximately equivalent to the maximum particle diameter. Based on these connectivity characteristic parameters, the proposed model is utilized to evaluate the ETCs for each structure, and the evaluated results are compared with those from simulations. The detailed comparison is listed in Table 3, where HJB denotes the Hasselman-John-Benvensite model and PRT denotes the presented connectivity model. The relative errors are calculated by:

$$\text{err} = \frac{|k_{\text{evaluated}} - k_{sim}|}{k_{sim}} \times 100\% \tag{24}$$

In all instances, the ETCs evaluated by the proposed model exhibit smaller relative errors in comparison to those obtained by the HJB model. Furthermore, the improvement observed on CR2 is larger than that on CR1, if the TCRs are considered.

The results indicate that the ETCs of CR1 and CR2 are larger than that of C1, with CR2 exhibiting the largest value. This observation can be attributed to the fact that, with the same particle number and the same

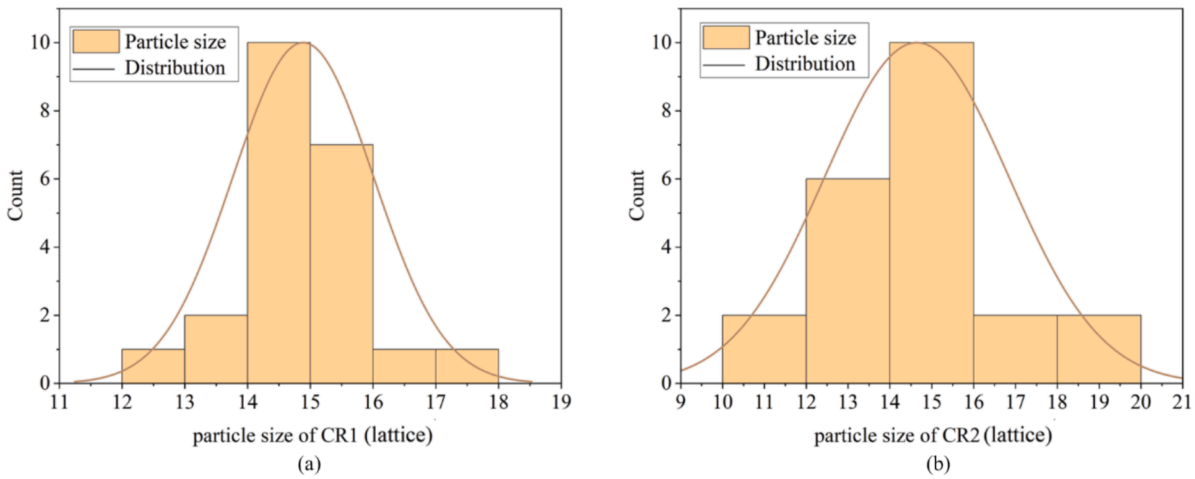

Fig. 8. Radius of randomly generated structures filled of particles with varying sizes.

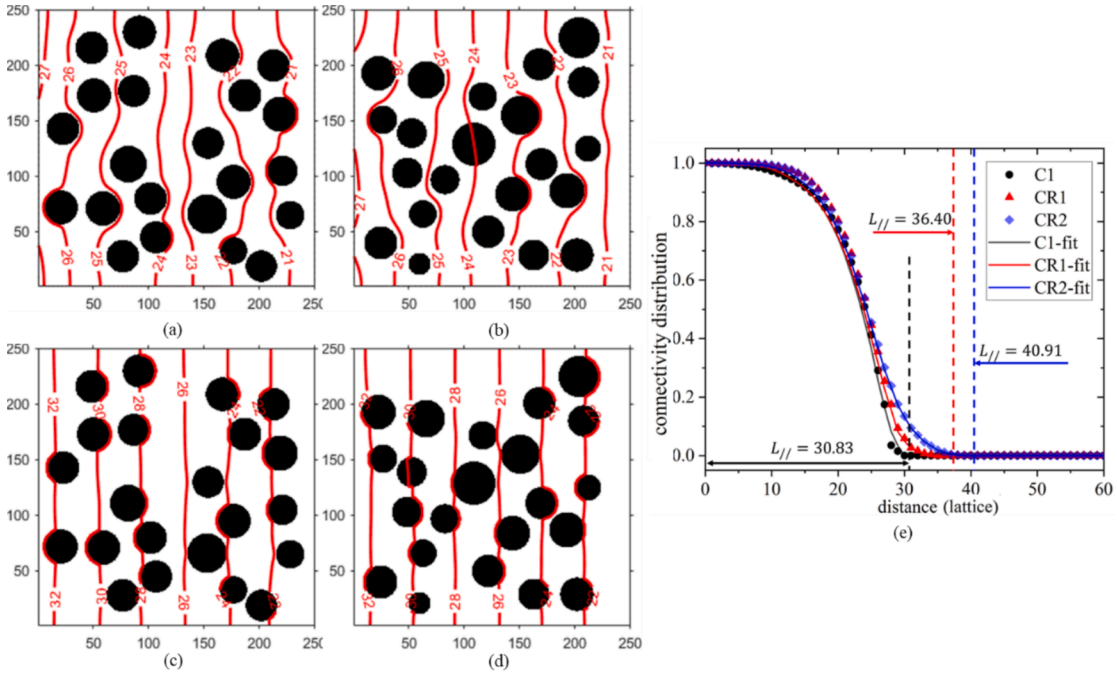

Fig. 9. Structures filled with particles with different size distributions and the corresponding simulation results: (a) for CR1 with $r_k = 0$ lattice; (b) for CR2 with $r_k = 0$ lattice; (c) for CR1 with $r_k = 26$ lattice; (d) for CR1 with $r_k = 26$ lattice. (e) comparison of the connectivity distributions of each structure.

Table 3
Comparison of ETCs evaluated by the proposed model and the HJB model.

r_k	C1			CR1					CR2				
	sim	HJB	err	sim	HJB	err HJB	PRT	err PRT	sim	HJB	err HJB	PRT	err PRT
0	1.68	1.64	2.8 %	1.69	1.64	3.5 %	1.64	3.5 %	1.72	1.65	4.0 %	1.65	4.0 %
7.5	1.25	1.17	5.8 %	1.25	1.17	5.9 %	1.22	2.2 %	1.26	1.18	6.4 %	1.25	0.5 %
15	1.07	1.00	6.7 %	1.07	1.00	6.8 %	1.04	2.6 %	1.07	1.00	7.2 %	1.07	0.3 %
26	0.94	0.88	6.4 %	0.93	0.88	6.2 %	0.91	2.1 %	0.94	0.87	7.1 %	0.94	0.5 %
39	0.85	0.80	5.5 %	0.85	0.80	6.0 %	0.83	2.4 %	0.86	0.80	6.5 %	0.85	0.6 %
45	0.82	0.78	5.1 %	0.82	0.78	5.1 %	0.81	1.6 %	0.83	0.78	6.2 %	0.82	0.6 %

mean radii, the varying particle size leads to an increased particle volume fraction. It can be explained mathematically with a simple statistical analysis:

if $\frac{1}{nb}\sum_{i=1}^{nb} r_{CR,i} = r_C$, $\cdot\frac{1}{nb}\sum_{i=1}^{nb} r_{CR,i}^2 \geq r_c^2$

with *nb* present the total number of particles. In this test, the volume fractions are 24.53 %, 24.61 %, and 25.16 % for samples of C1, CR1, and CR2, respectively. Conversely, when the particle volume fraction is the same, the average radius in cases with varying particle sizes is smaller than that of the uniform case. As discussed in section 3.2 regarding the influence of varying particle sizes, this phenomenon will lead to a larger ETC considering a larger TCR. This trend could be also identified by

comparing the HJB evaluations and the proposed evaluations under the same volume fraction in Table.3.

Based on these theoretical and numerical analyses, the statistical maximum radius, rather than the average radius, is recommended for a more accurate evaluation of ETCs of structures containing particles of varying sizes.

4.2. PFS structures with fillers of different orientation

The elliptical fillers characterized by the same shape parameter as listed in Table 2 are examined in this study. The ratio of the major to minor axis is 3, with the length of the minor axis equals to the diameter of the smallest circular filler depicted in Fig. 6 (C1). Additionally, the equal area effective radius (r21) is equal to the radius of the medium size circular filler (C2). Three distinct orientation distributions, denoted as E1, E2, and E3, respectively, are analyzed. The particle volume fraction is 23.8 % for both E1 and E2 and is 23.6 % for E3. Fig. 10 shows two typical simulation results for these three structures with r_k equals 0 and 26 lattice.

The connectivity distribution function for the circular and elliptical structures is calculated for ETC evaluation with the proposed models as shown in Fig. 11. In scenarios where particles are arranged in the same orientation, the characteristic length of the connectivity is as approximately equivalent to the diameter of the circular particle or the length of the axis along the heat flux of the elliptical particle, as explained in section 2.1 and 2.4. A notable distribution feature is observed for C3, which includes only four particles in the structure, resulting a lack of statistical reliability. For configuration E3 where each elliptical particle is oriented randomly, the connectivity function resembles a Gaussian distribution, thus a data fitting is utilized to assess the connectivity characteristic length of as illustrated in Fig. 11(a).

In order to compare the effects of particle shape and orientation on ETCs, the simulated and evaluated results are presented in Fig. 11(b). The relative errors between the ETCs predicted by different models and the numerical simulation results are listed in Table 4. The results indicate that particle shape exerts a larger influence on ETCs than particle size. The significant changes associated with the shape and orientation of fillers can be characterized by the proposed model. The predicted ETCs for E1 and E3 closely align with the results of numerical simulations. Both models have a large underestimation for E2, and the accuracy of the predictions using the proposed method is also improved. The proposed model explains this phenomenon through Eq.(14) as a larger connectivity along the heat flux direction enhances heat transfer and reduces the obstruction of TCRs resulting in a larger ETC. The definition of dimensionless thermal barrier resistance using the connectivity length Eq.(14), different from the definition using an effective radius presented in Eq.(6), not only clears up the confusion about which kind of effective radius should be used, but also provides a easily accessible quantitative parameter for structures containing particles with varying orientations.

Furthermore, the ETCs of E1 is slightly smaller than those of C1, particularly when considering TCRs. Similarly, the ETCs of E3 is slightly smaller than those of C2. This observation can be straightforwardly explained by the morphological parameter proposed f in this work. As illustrated in in Fig. 11(a), a comparison between C1 and E1 reveals that their connectivity functions are almost the same along the heat flux, while the connectivity of E1 is larger than that of C1 in the direction perpendicular to the heat flux. A comparable trend is observed for C2 and E3, where their connectivity functions are relatively similar along the heat flux direction, yet the connectivity of E3 is slightly larger than that of C2 in the direction perpendicular to the heat flux. This establishes

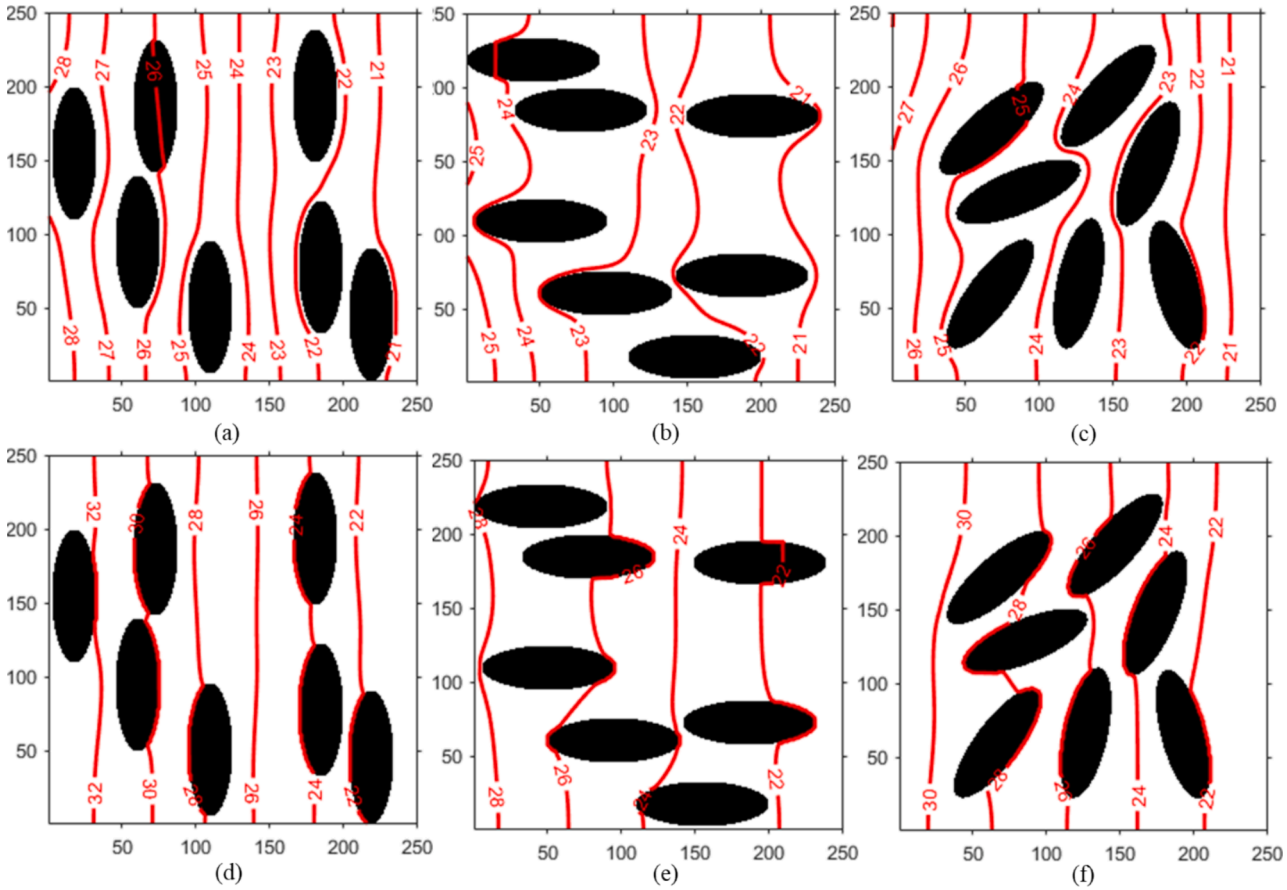

Fig. 10. Structures filled with elliptical particles with different orientation distribution and corresponding simulation results: (a) for E1 with$r_k = 0$ lattice; (b) for E2 with$r_k = 0$ lattice; (c) for E3 with$r_k = 0$ lattice; (d) for E1 with $r_k = 26$ lattice; (e) for E2 with $r_k = 26$ lattice; (f) for E3 with $r_k = 26$ lattice.

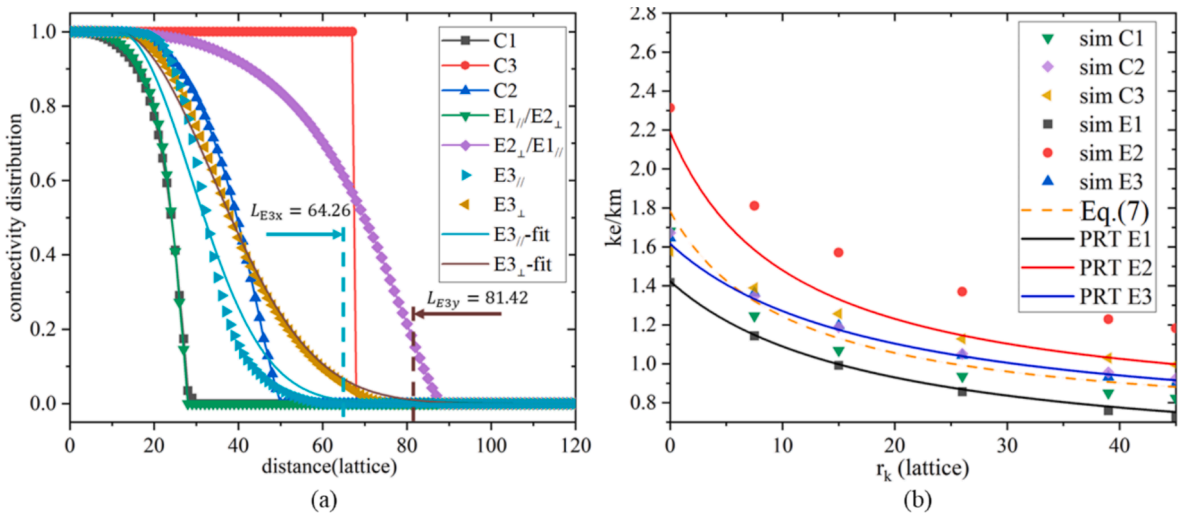

Fig. 11. (a) Comparison of the connectivity distributions functions of structure filled with circular and elliptical particles; (b) Comparison of ETCs simulated and evaluated using the proposed model and Eq.(7).

Table 4
Comparison of ETCs evaluated by the proposed model and the model Eq.(7) for structures with fillers of different orientation.

r_k	E1					E2				E3			
	Eq.(7)	sim	errEq.(7)	PRT	errPRT	Sim	errEq.(7)	PRT	errPRT	Sim	errEq.(7)	PRT	ErrPRT
0	1.78	1.42	25.4 %	1.42	0.4 %	2.31	22.9 %	2.19	5.2 %	1.65	7.9 %	1.62	1.8 %
7.5	1.32	1.14	15.8 %	1.15	0.9 %	1.81	27.1 %	1.59	12.1 %	1.36	2.9 %	1.34	1.5 %
15	1.13	0.99	14.1 %	1	1.0 %	1.57	28.0 %	1.33	15.3 %	1.19	5.0 %	1.18	0.8 %
26	0.99	0.86	15.1 %	0.87	1.1 %	1.37	27.7 %	1.15	16.1 %	1.04	4.8 %	1.04	0.2 %
39	0.91	0.76	19.7 %	0.78	2.6 %	1.23	26.0 %	1.03	16.2 %	0.93	2.2 %	0.94	1.1 %
45	0.88	0.73	20.6 %	0.75	2.7 %	1.18	25.4 %	1.00	15.3 %	0.89	1.1 %	0.91	2.2 %

a clear relationship between ETC and connectivity, indicating that the connectivity length along heat flux reflects the influence of TRCs and the ratio of connectivity length in orthogonal directions reflects the influences of shape and orientation, as articulated by the proposed model in Eq.(14) and Eq.(16).

The impact of the connectivity-based model on various kp/km ratios is discussed based on structure E3. Fig. 12 compares the simulated and evaluated ETCs for the kp/km ratios of 10, 100, and 1000, and Table 5 compares the relative errors between the ETCs predicted by different

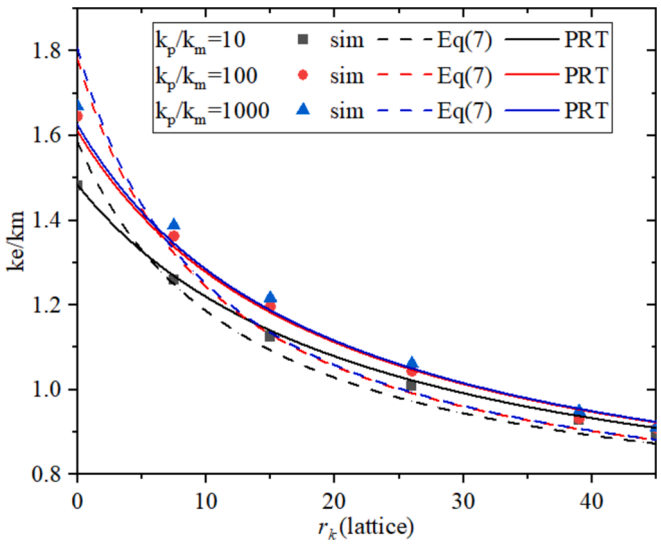

Fig. 12. Comparison of ETCs simulated and evaluated using the proposed model under various kp/km ratio.

models and the numerical simulation results. It shows that the evaluated results match well with the simulation results and the proposed connectivity model obtains closer results to the simulation results compared with the classical model expressed by Eq.(7) for all cases. The ETCs under the ratio of 100 and 1000 are close, but they are quite different from that under the ratio of 10, in both the simulation and evaluated results. These observations are consistent with the previous literatures (Zhou and Cheng 2014, Rao et al., 2017), whereas kp/km ratio of 100 is optimal for effectively illustrating the influence of high thermal conductivity particles with reasonable computational effort in numerical studies. Accordingly, the ratio of 100 is generally adopted in this work.

Then the effect of particle volume fraction is discussed. Two structures are generated by randomly selecting several particles from structure E3, as shown in Fig. 13(a) and (b). By selecting 3 and 5 particles, the corresponding volume fractions are 9.7 % and 16.2 % respectively. The simulated and evaluated ETCs are compared in Fig. 13(c). The relative errors between the ETCs predicted by different models and the numerical simulation results are listed in Table 6. As the volume fraction increases, the errors between simulation results and evaluated results by Eq.(7) increases, which consistent with the assumption of the Maxwell-type model that the particles should be discrete and far apart. In contrast, the ETCs evaluated using the proposed model demonstrate a strong agreement with the simulation results for all three cases.

4.3. *PFS structures with fillers of irregular shape*

To assess the generalizability of the proposed model, the ETCs of structures filled with irregular fillers, which are challenging to evaluate directly using other analytical models are investigated. This section focuses on two typical types of irregular fillers known as the isotropic and the fibrous particles.

Four detailed microstructures have been reconstructed based on the

Table 5
Comparison of ETCs evaluated by the proposed model and the model Eq.(7) for various kp/km ratio.

	kp/km = 10					kp/km = 100					kp/km = 1000				
r_k	sim	Eq(7)	errEq(7)	PRT	err PRT	Sim	Eq(7)	errEq(7)	PRT	err PRT	sim	Eq(7)	errEq(7)	PRT	err PRT
0	1.48	1.59	7.0 %	1.48	0.2 %	1.65	1.78	8.2 %	1.61	2.1 %	1.67	1.81	8.2 %	1.63	2.6 %
7.5	1.26	1.25	0.9 %	1.27	0.7 %	1.36	1.32	3.0 %	1.34	1.8 %	1.39	1.33	4.1 %	1.35	3.1 %
15	1.13	1.09	2.9 %	1.14	1.2 %	1.20	1.13	5.4 %	1.18	1.1 %	1.22	1.14	6.7 %	1.19	2.4 %
26	1.01	0.97	3.5 %	1.02	1.4 %	1.04	0.99	5.0 %	1.05	0.4 %	1.06	0.99	6.4 %	1.05	1.1 %
39	0.93	0.90	3.4 %	0.94	1.1 %	0.93	0.91	2.7 %	0.95	2.3 %	0.95	0.91	4.4 %	0.96	0.6 %
45	0.90	0.87	2.6 %	0.91	1.5 %	0.91	0.88	3.1 %	0.92	1.5 %	0.91	0.88	3.3 %	0.92	1.4 %

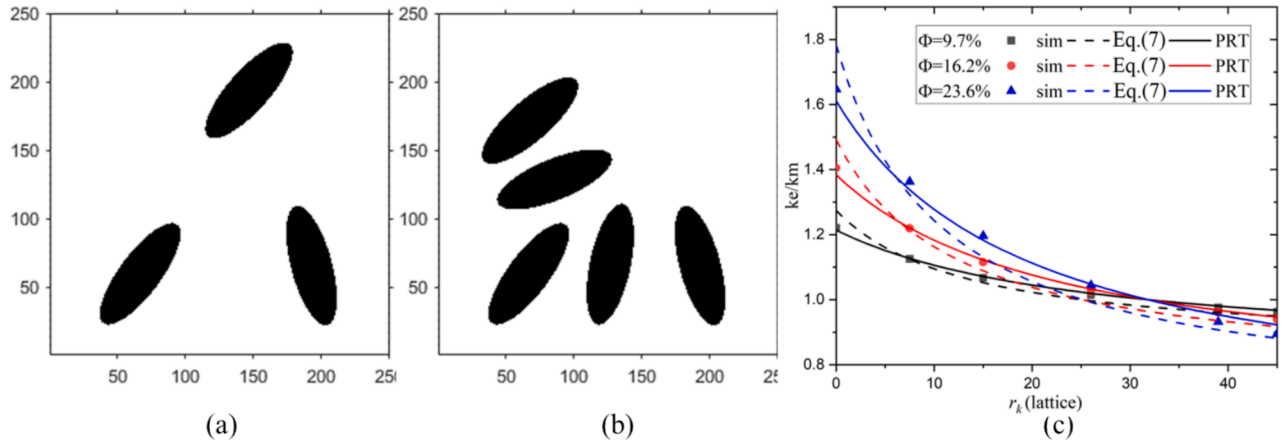

Fig. 13. Comparison of ETCs simulated and evaluated by the proposed model under various particle volume fraction.

Table 6
Comparison of ETCs evaluated by the proposed model and the model Eq.(7) for various particle volume fraction.

r_k	Φ=9.7 %					Φ=16.2 %					Φ=23.6 %				
	sim	Eq(7)	errEq(7)	PRT	err PRT	Sim	Eq(7)	errEq(7)	PRT	err PRT	sim	Eq(7)	errEq(7)	PRT	err PRT
0	1.22	1.27	4.4 %	1.21	0.5 %	1.41	1.49	6.2 %	1.38	1.5 %	1.65	1.78	8.2 %	1.61	2.1 %
7.5	1.13	1.12	0.1 %	1.13	0.1 %	1.22	1.21	0.5 %	1.22	0.1 %	1.36	1.32	3.0 %	1.34	1.8 %
15	1.07	1.05	1.4 %	1.07	0.4 %	1.12	1.09	2.4 %	1.12	0.6 %	1.20	1.13	5.4 %	1.18	1.1 %
26	1.01	1.00	1.7 %	1.02	0.5 %	1.02	0.99	3.0 %	1.03	0.8 %	1.04	0.99	5.0 %	1.05	0.4 %
39	0.98	0.96	1.5 %	0.98	0.5 %	0.96	0.94	2.7 %	0.97	0.7 %	0.93	0.91	2.7 %	0.95	2.3 %
45	0.96	0.95	1.4 %	0.97	0.5 %	0.94	0.92	2.4 %	0.95	0.7 %	0.91	0.88	3.1 %	0.92	1.5 %

work of Su et al. (Su et al., 2017). Fig. 14(a) and (b) illustrate isotropic cases with particle volume fraction of 19.35 % and 26.24 %, denoted as A1 and A2. Additionally, two fibrous structures, referred to as F1 and F2, exhibit particle volume fractions of 10 % and 25 % as shown in Fig. 14(c) and (d). These structures are randomly cut from cross-sections of the 3D generation displayed in Su et al.'s work, and a post-processing known as direct sampling (Mariethoz and Renard 2010) is applied to reconstruct the fibrous structures while controlling the volume fraction. The direct sampling method identifies a given particle-filled structure and randomly sampling same of the particles to generate new structures. This method is a widely used structure reconstruction tool in spatial statistics and has been proven able to keep statistical consistence. Based on this theory, the connectivity functions calculated based on F2 can be utilized for both F1 and F2 in this paper. This treatment eliminates bias of the directly calculating from structure F1, where the number of fillers is too small to satisfy the statistical demands. The calculated and fitted connectivity functions for these cases are displayed in Fig. 14(e).

It shows that the connectivity distribution along the x- and y-axis exhibits minimal variation for each isotropic structure, which is a distinct statistical characteristic of isotropic distributions. The different connectivity characteristic lengths correspond to the different structures A1 and A2. Consequently, the isotropic irregular particles can be regarded as circular particles (or as elliptical particles with a small ratio of major to minor axes, which yield very similar results in these two instances) to evaluate the ECTs by the proposed connectivity-based model. For fibrous structures, a higher connectivity along the x-axis is obtained. Since cylindrical fibers are assumed in the referenced 3D structure, the reconstructed 2D particles are assumed to be rectangular for the ETC evaluation. The proposed model is then utilized to predict the ETCs of the isotropic structures along the x-axis and those of the fibrous structures along both x- and y-axes. In contrast, due to the absence of prior information of the irregular particles, previous models have difficulties in determining the effective diameters and orientation distributions for the evaluation of ETCs. Thus, Fig. 15 simply compares the results evaluated by the proposed model with simulation results, and the corresponding relative errors are displayed in Table 7.

Overall, the predicted results are in agreement with the simulation results. The relative errors are typically in the range from 0 to 14.7 %. We argued that such large relative errors might be due to the highly complex geometry structures and the simplified approximation of the numerical models. The LBM model utilizes an approximation to assign the components within each computational grid and generate a stair-like interface boundary (Li et al., 2021a). This approximation may introduce errors at curved particle–matrix interfaces, potentially reducing the accuracy of simulations in systems filled with irregular particles in these tests, where highly complex structures are present. In addition, another two structures, an isotropic one with a volume fraction of 38.6 % and a fibrous one with a volume fraction of 35.0 %, are evaluated using the

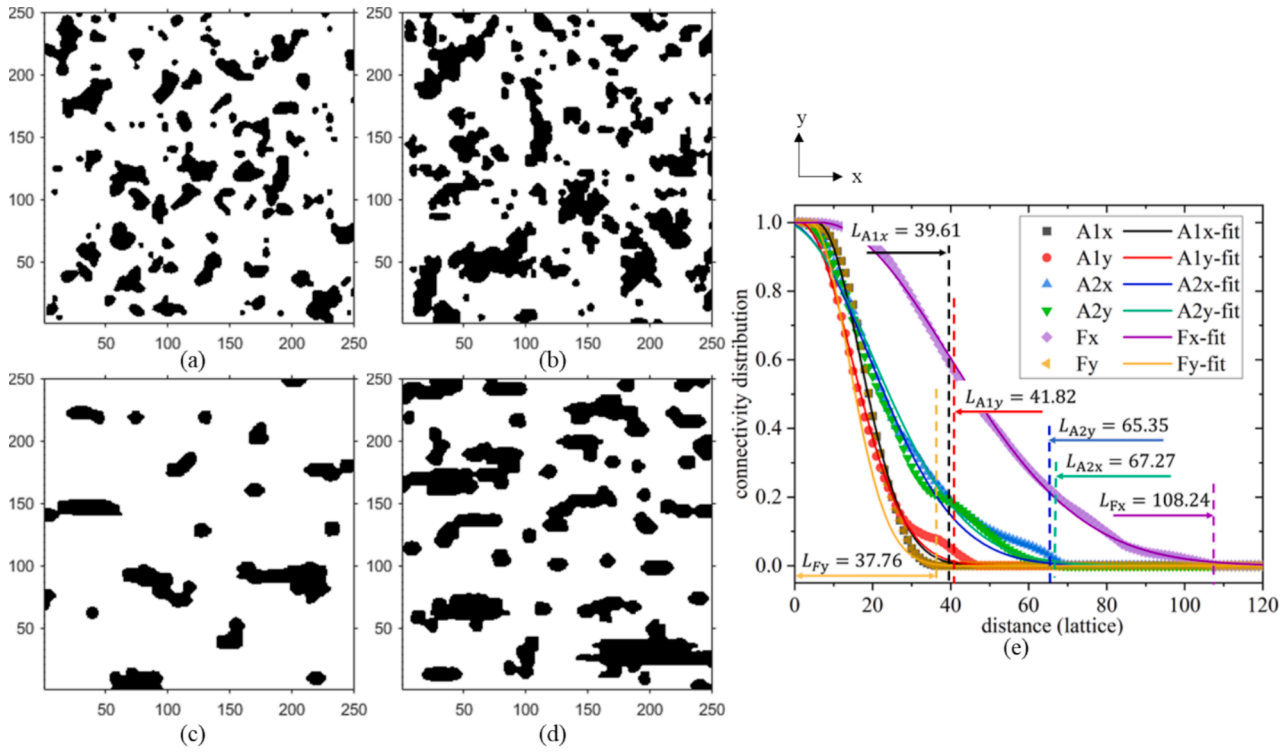

Fig. 14. The irregular particle-filled structures and the corresponding treatment for connectivity characteristic length: (a)-(b) isotropic; (c)-(d) fibrous; (e) calculated and fitted connectivity distributions for each structure.

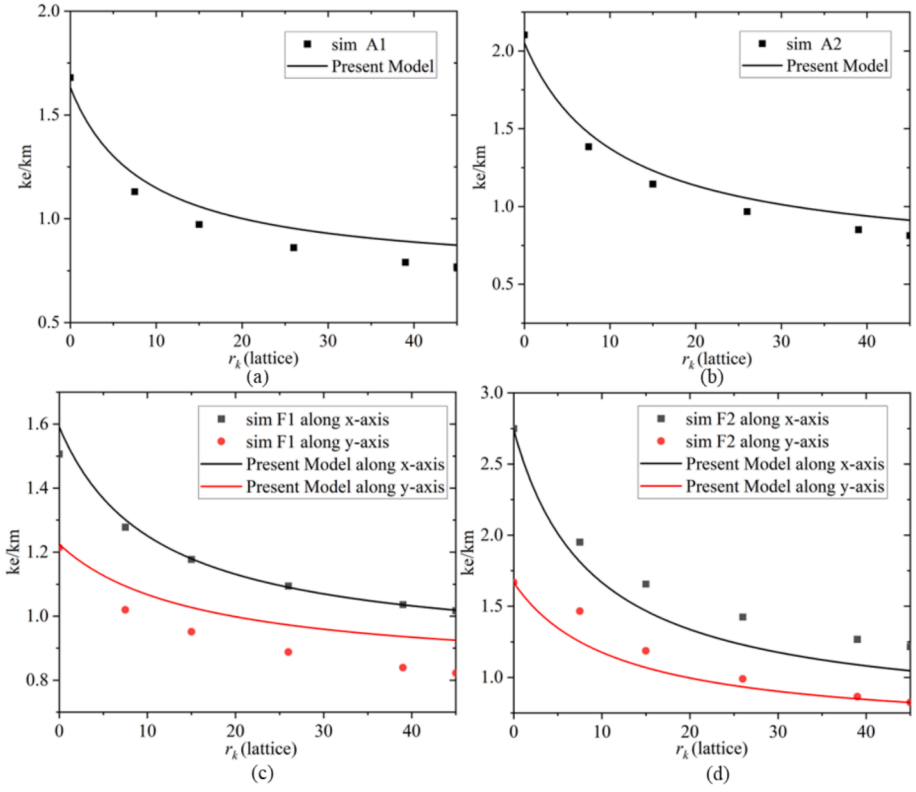

Fig. 15. Predict the ETCs of structures filled with irregular particles utilizing the proposed model and compare with simulation results.

proposed method. The relative errors observed in these two cases were significant, with the maximum error of 17.8 % and 22.3 %, respectively. The results are deemed insufficient and are not presented in this paper.

It can be concluded that the connectivity characteristic length effectively captures the obstruction effects of thermal resistances associated with irregular particles. For the non-isotropic structures, the

Table 7
The relative errors between the ETCs evaluated by the proposed model and numerical simulations for irregular particle filled structures.

r_k		0	7.5	15	26	39	45
A1	sim	1.68	1.13	0.97	0.86	0.79	0.77
	PRT	1.63	1.21	1.06	0.95	0.89	0.87
	err	2.8 %	7.4 %	9.0 %	10.8 %	12.8 %	13.6 %
A2	sim	2.10	1.38	1.14	0.97	0.85	0.81
	PRT	2.05	1.47	1.23	1.05	0.95	0.91
	err	2.4 %	6.4 %	7.6 %	8.9 %	11.1 %	12.2 %
F1-x	sim	1.51	1.28	1.18	1.09	1.04	1.02
	PRT	1.59	1.30	1.18	1.09	1.04	1.02
	err	5.6 %	1.8 %	0.2 %	0.3 %	0.1 %	0.2 %
F1-y	sim	1.21	1.02	0.95	0.89	0.84	0.82
	PRT	1.22	1.09	1.03	0.97	0.94	0.92
	err	0.9 %	7.3 %	8.0 %	9.5 %	11.6 %	12.5 %
F2-x	sim	2.75	1.95	1.66	1.42	1.27	1.22
	PRT	2.74	1.81	1.47	1.23	1.09	1.05
	err	0.3 %	7.1 %	11.4 %	13.7 %	14.1 %	13.9 %
F2-y	sim	1.67	1.47	1.19	0.99	0.86	0.82
	PRT	1.67	1.25	1.07	0.93	0.85	0.82
	err	0.0 %	14.7 %	9.9 %	5.7 %	1.7 %	0.1 %

orientation relevant connectivity directly incorporates the influence of orientation. Compared to classical theoretical models, the proposed model provides a consistent treatment process for structures filled with a diverse range of fillers, including irregular ones. However, as an extension of the Maxwell model, the proposed model is appropriate for systems with a low particle volume fraction, specifically those below approximately 25 %.

4.4. Three dimensional applications

In this section, a three-dimensional (3D) PFS filled with randomly distributed ellipsoidal particles is investigated. As illustrated in Fig. 16 (a), eleven ellipsoids with semi-axes measuring 15, 25, and 45 lattice are randomly distributed within a 200 × 200 × 200 computational lattice. The particle volume fraction is 9.7 %. The ETCs along the x, y, and z axes under varying TCRs are simulated. The simulated temperature equivalent surfaces under $r_k = 26$ lattice for each direction are displayed in Fig. 16(d)-(f). The connectivity characteristic lengths along these three directions are fitted and displayed shown in Fig. 16(b). For the ETCs along x-direction, the connectivity characteristic length along heat flux is clear, that is,

$$L_{//} = L_x$$

and the connectivity perpendicular to this direction can be defined as:

$$L_{\perp} = \sqrt{L_y L_z}$$

This definition is applied to all directions. It is important to highlight that the complete 3D structure is not necessary for the calculation of connectivity distribution functions. Two arbitrarily selected slices, one along with the study direction and the other perpendicular to it, are adequate to derive the corresponding characteristic lengths for ETC evaluation. These attributes enable the proposed connectivity model to demonstrate considerable efficiency in 3D applications.

Subsequently, the predicted ETCs are compared with the simulated results, revealing good agreements across all directions, as illustrated in Fig. 16(c). The detailed relative errors are listed in Table 8. The results show comparable errors for the two evaluation models along x-direction, and much smaller relative errors with the proposed model along y- and z-direction. The proposed model can accurately and efficiently evaluate the ETCs of 3D anisotropic structures. This is achieved through the connectivity distribution function, which directly captures the arrangement characteristics of non-spherical filled systems.

5. Conclusions

A connectivity model is developed to predict the effective thermal

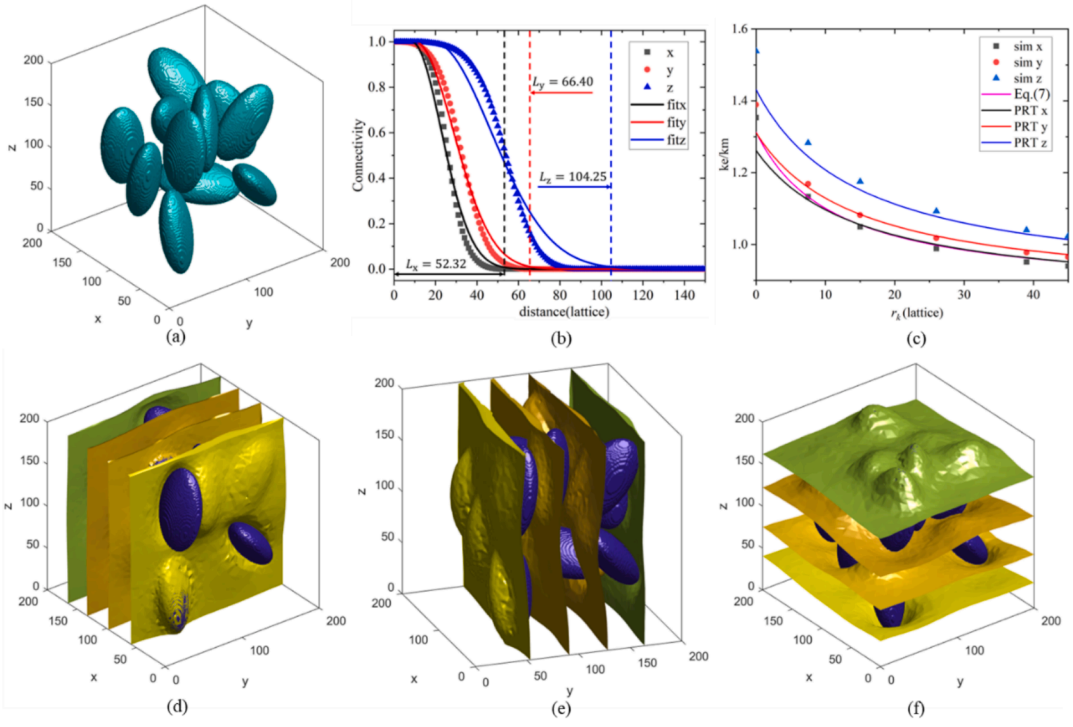

Fig. 16. ETCs of a 3D structure filled with randomly distributed ellipsoidal particles. (a) structure; (b) connectivity distribution curve along three directions; (c) comparison of simulated and evaluated ETCs; (d)-(f) simulation results under kp/km = 100 and $r_k = 26$ lattice shown by temperature equivalent-surfaces with heat flux along x, y, and z axes.

Table 8
Comparison of ETCs evaluated by the proposed model and the model Eq.(7) for 3D structure.

r_k	x-direction					y-direction				z-direction			
	Eq.(7)	Sim	errEq.(7)	PRT	errPRT	Sim	errEq.(7)	PRT	errPRT	Sim	errEq.(7)	PRT	ErrPRT
0	1.31	1.35	3.0 %	1.26	6.5 %	1.39	5.5 %	1.31	5.6 %	1.54	14.7 %	1.43	7.0 %
7.5	1.13	1.13	0.1 %	1.12	0.8 %	1.17	3.1 %	1.16	0.8 %	1.28	11.7 %	1.24	3.0 %
15	1.05	1.05	0.6 %	1.06	0.6 %	1.08	2.5 %	1.08	0.2 %	1.18	10.2 %	1.15	2.0 %
26	1.00	0.99	1.3 %	1.00	1.1 %	1.02	1.9 %	1.02	0.6 %	1.09	8.7 %	1.08	1.4 %
39	0.96	0.95	1.2 %	0.96	1.2 %	0.98	1.5 %	0.98	0.7 %	1.04	7.5 %	1.03	1.1 %
45	0.95	0.94	1.2 %	0.95	1.2 %	0.97	1.4 %	0.97	0.7 %	1.02	7.0 %	1.01	1.0 %

conductivity of particle-filled systems considering interfacial resistance. By applying spatial statistics theory, the optimized heat flow path is obtained in terms of connectivity distribution from the geometric structures of PFS directly, without the necessity to consider the specific size, shape, and orientation of individual particles. By analyzing Maxwell-type models and fitting LBM simulation results across various PFS structures, concise connectivity characteristic lengths were utilized to describe PFS structures and to construct the proposed model. The proposed model quantitatively interprets the influence of diverse typical particles on the ETCs reported in the literature.

This study investigates structures commonly encountered in practical applications, specifically the PFSs containing particles of varying sizes, random orientations, and irregular shapes in both 2D and 3D contexts through theoretical and numerical analyses. The ETCs predicted by the proposed model demonstrate strong agreement with simulation results for PFS structures exhibiting a particle-to-matrix thermal conductivity ratio lower 1000 and a particle volume fraction lower than 25 %. However, we would stress that our proposed method should be used with caution as the particles presumably do not contact in the derivation of the model. In comparison to previous models, the proposed model provides more accurate evaluations of ETCs, as the connectivity characteristic lengths utilized in the model incorporate information about particle distribution in addition to particle shape factors. Furthermore, our approach generalizes the evaluation of systems filled with arbitrary shaped particles, significantly simplifying and harmonizing applications involving nonuniform and irregular particles, which is ambitious in practical situations. These findings suggest that the underlying structural information has the potential to construct a unified universal model. Additionally, in the present model we do not consider thermal radiation. Basically, the thermal radiation can affect ETCs and is closely related to the geometric structure of particle filled systems (Luo et al., 2022, Nee and Hussein 2024). The proposed model is based on spatial statistical methods which in principle can be used to account for the thermal radiation. The establishment of a robust characterization method and the construction of a cohesive model including thermal radiation will be the subject of future work.

CRediT authorship contribution statement

Xue Li: Writing – original draft, Validation, Software, Methodology, Investigation, Funding acquisition, Conceptualization. **Yiqi Song:** Writing – review & editing, Validation. **Mao Ye:** Writing – review & editing, Supervision, Resources, Project administration.

Declaration of competing interest

The authors declare that they have no known competing financial interests or personal relationships that could have appeared to influence the work reported in this paper.

Acknowledgments

This work was financially supported by the National Natural Science Foundation of China (Grant Number: 22108269 and 22293024) and the DICP Innovation Foundation (Grant Number: I202238).

Data availability

Data will be made available on request.

References

Agari, Y., Uno, T., 1986. Estimation on thermal conductivities of filled polymers. J. Appl. Polym. Sci. 32 (7), 5705–5712.
Benveniste, Y., 1987. Effective thermal conductivity of composites with a thermal contact resistance between the constituents: nondilute case. J. Appl. Phys. 61 (8), 2840–2843.
Birkholz, O., Gan, Y., Kamlah, M., 2019. Modeling the effective conductivity of the solid and the pore phase in granular materials using resistor networks. Powder Technol. 351, 54–65.
Bruggeman, D. A. G. (1935). "Berechnung verschiedener physikalischer Konstanten von heterogenen Substanzen. I. Dielektrizitätskonstanten und Leitfähigkeiten der Mischkörper aus isotropen Substanzen." 416(8): 665-679.
Caers, J., 2011. Modeling uncertainty in the earth sciences. John Wiley & Sons.
Carson, J.K., Lovatt, S.J., Tanner, D.J., Cleland, A.C., 2005. Thermal conductivity bounds for isotropic, porous materials. Int. J. Heat Mass Transf. 48 (11), 2150–2158.
Chen, L., Wang, C., Moscardini, M., Kamlah, M., Liu, S., 2019. A DEM-based heat transfer model for the evaluation of effective thermal conductivity of packed beds filled with stagnant fluid: Thermal contact theory and numerical simulation. Int. J. Heat Mass Transf. 132, 331–346.
Chu, K., Li, W.-S., Tang, F.-L., 2013. Flatness-dependent thermal conductivity of graphene-based composites. Phys. Lett. A 377 (12), 910–914.
Deissler, R. G. and J. S. J. J. o. F. E. Boegli (1958). "An Investigation of Effective Thermal Conductivities of Powders in Various Gases.".
del Río, J.A., Zimmerman, R.W., Dawe, R.A., 1998. Formula for the conductivity of a two-component material based on the reciprocity theorem. Solid State Commun. 106 (4), 183–186.
Dhaidan, N.S., Kokz, S.A., Rashid, F.L., Hussein, A.K., Younis, O., Al-Mousawi, F.N., 2022. Review of solidification of phase change materials dispersed with nanoparticles in different containers. J. Storage Mater. 51, 104271.
El Mansouri, A., Hasnaoui, M., Amahmid, A., Alouah, M., 2020. Numerical analysis of conjugate convection-conduction heat transfer in an air-filled cavity with a rhombus conducting block subjected to subdivision: cooperating and opposing roles. Int. J. Heat Mass Transf. 150, 119375.
Every, A.G., Tzou, Y., Hasselman, D.P.H., Raj, R., 1992. The effect of particle size on the thermal conductivity of ZnS/diamond composites. Acta Metall. Mater. 40 (1), 123–129.
Fan, J., Wang, L., 2011. Review of heat conduction in nanofluids. J. Heat Transfer 133 (4).
Florio, L.A., 2018. Development of novel heat conduction interaction model for solid body thermal contact in CFD based particle flow simulations. Chem. Eng. Sci. 192, 448–466.
Fricke, H., 1953. The Maxwell-Wagner dispersion in a suspension of ellipsoids. J. Phys. Chem. 57 (9), 934–937.
Gao, B.Z., Xu, J.Z., Peng, J.J., Kang, F.Y., Du, H.D., Li, J., Chiang, S.W., Xu, C.J., Hu, N., Ning, X.S., 2015. Experimental and theoretical studies of effective thermal conductivity of composites made of silicone rubber and Al_2O_3 particles. Thermochim Acta 614, 1–8.
Gharagozloo-Hubmann, K., A. Boden, G. J. F. Czempiel, I. Firkowska, S. Reich (2013). "Filler geometry and interface resistance of carbon nanofibres: Key parameters in thermally conductive polymer composites." 102(21): 213103.
Goovaerts, P., 1998. Geostatistical tools for characterizing the spatial variability of microbiological and physico-chemical soil properties. Biol. Fertil. Soils 27 (4), 315–334.
Guo, Z., Sun, Z., Zhang, N., Ding, M., Shi, S., 2019. CFD analysis of fluid flow and particle-to-fluid heat transfer in packed bed with radial layered configuration. Chem. Eng. Sci. 197, 357–370.
Hamilton, R.L., Crosser, O.K., 1962. Thermal conductivity of heterogeneous two-component systems. Ind. Eng. Chem. Fundam. 1 (3), 187–191.
Hashin, Z., Shtrikman, S., 1962. A variational approach to the theory of the effective magnetic permeability of multiphase materials. J. Appl. Phys. 33 (10), 3125–3131.
Hasselman, D.P.H., Johnson, L.F., 1987. Effective thermal conductivity of composites with interfacial thermal barrier resistance. J. Compos. Mater. 21 (6), 508–515.
Hsu, C.T., Cheng, P., Wong, K.W., 1995. A lumped-parameter model for stagnant thermal conductivity of spatially periodic porous media. J. Heat Transfer 117 (2), 264–269.

Jiajun, W., Xiao-Su, Y., 2004. Effects of interfacial thermal barrier resistance and particle shape and size on the thermal conductivity of AlN/PI composites. Compos. Sci. Technol. 64 (10), 1623–1628.
Journel, A. G. (1993). Geostatistics: roadblocks and challenges. Geostatistics Troia'92, Springer: 213-224.
Kapitza, P.L., 1941. Heat Transfer and Superfluidity of Helium II. Phys. Rev. 60 (4), 354–355.
Ke, X., Duan, Y., 2019. A spatially-varying relaxation parameter Lattice Boltzmann Method (SVRP-LBM) for predicting the effective thermal conductivity of composite material. Comput. Mater. Sci 169, 109080.
Klise, K.A., Weissmann, G.S., McKenna, S.A., Nichols, E.M., Frechette, J.D., Wawrzyniec, T.F., Tidwell, V.C., 2009. Exploring solute transport and streamline connectivity using lidar-based outcrop images and geostatistical representations of heterogeneity. Water Resour. Res. 45 (5).
Landauer, R., 2004. The electrical resistance of binary metallic mixtures. J. Appl. Phys. 23 (7), 779–784.
Li, X., G. Mariethoz, D. Lu and N. Linde (2016). "Patch-based iterative conditional geostatistical simulation using graph cuts." 52(8): 6297-6320.
Li, X., Gao, D., Hou, B., Wang, X., 2021a. An inserted layer LBM for thermal conduction with contact resistances. Chem. Eng. Sci. 233, 116431.
Li, Y., Tan, Z., Zhang, Q., Liu, X., Chen, J., Yao, J., 2021b. Refining the concept of hydrological connectivity for large floodplain systems: Framework and implications for eco-environmental assessments. Water Res. 195, 117005.
Li, L., Zheng, H., Yuan, C., Hu, R., Luo, X., 2016a. Study on effective thermal conductivity of silicone/phosphor composite and its size effect by Lattice Boltzmann method. Heat Mass Transf. 52 (12), 2813–2821.
Liang, Y., Li, X., 2014. A new model for heat transfer through the contact network of randomly packed granular material. Appl. Therm. Eng. 73 (1), 984–992.
Lipton, R., 1997. Variational methods, bounds, and size effects for composites with highly conducting interface. J. Mech. Phys. Solids 45 (3), 361–384.
Luo, M., Wang, C., Zhao, J., Liu, L., 2022. Characteristics of effective thermal conductivity of porous materials considering thermal radiation: a pore-level analysis. Int. J. Heat Mass Transf. 188, 122597.
Mariethoz, G., Caers, J., 2014. Multiple-point Geostatistics: Stochastic Modeling with Training Images. John Wiley & Sons.
Mariethoz, G., Renard, P., 2010. Reconstruction of incomplete data sets or images using direct sampling. Math. Geosci. 42 (3), 245–268.
Maxwell, J.C., 1904. A Treatise on Electricity and Magnetism. Clarendon Press.
Mori, T., Tanaka, K., 1973. Average stress in matrix and average elastic energy of materials with misfitting inclusions. Acta Metall. 21 (5), 571–574.
Nan, C.-W., Birringer, R., Clarke, D.R., Gleiter, H., 1997. Effective thermal conductivity of particulate composites with interfacial thermal resistance. J. Appl. Phys. 81 (10), 6692–6699.
Nan, C.-W., Li, X.-P., Birringer, R., 2000. Inverse problem for composites with imperfect interface: determination of interfacial thermal resistance. Therm. Conductivi. Constituents, Microstructural Parameters 83 (4), 848–854.
Nee, A., Hussein, A.K., 2024. Hybrid Lattice Boltzmann Method for 3D Natural Convection Combined with Volumetric Radiation. J. Eng. Phys. Thermophys. 97 (3), 766–773.
Ngo, I.-L., Byon, C., 2015. A generalized correlation for predicting the thermal conductivity of composite materials. Int. J. Heat Mass Transf. 83, 408–415.
Ngo, I.-L., Jeon, S., Byon, C., 2016. Thermal conductivity of transparent and flexible polymers containing fillers: a literature review. Int. J. Heat Mass Transf. 98, 219–226.
Pietschak, A., Dixon, A.G., Freund, H., 2020. A new heat transfer correlation suited for the design of fixed-bed reactors via numerical optimization. Chem. Eng. Sci. 220, 115614.
Polansky, J., Jeffers, N., Punch, J., 2020. A hybrid approach for predicting the effective thermal conductivity of sintered porous materials. Int. J. Therm. Sci. 148, 106135.
Qin, X., Yin, W., 2023. A novel fractal model for effective thermal conductivity in granular porous media. Geothermics 108, 102625.
Rao, Z., Chen, B., Zhao, J., 2017. A series of generalized correlations for predicting the thermal conductivity of composite materials packing with artificially designed filler shapes. Appl. Therm. Eng. 120, 444–452.
Rashid, F. L., A. K. Hussein, E. H. Malekshah, A. Abderrahmane, K. Guedri and O. Younis (2022). "Review of Heat Transfer Analysis in Different Cavity Geometries with and without Nanofluids." 12(14): 2481.
Rodrigues, S.J., Vorhauer-Huget, N., Tsotsas, E., 2022. Effective thermal conductivity of packed beds made of cubical particles. Int. J. Heat Mass Transf. 194, 122994.
Rodrigues, S.J., Vorhauer-Huget, N., Tsotsas, E., 2023. Prediction of effective thermal conductivity of packed beds of polyhedral particles. Powder Technol. 430, 118997.
Rong, F., Zhang, W., Shi, B., Guo, Z., 2014. Numerical study of heat transfer enhancement in a pipe filled with porous media by axisymmetric TLB model based on GPU. Int. J. Heat Mass Transf. 70, 1040–1049.
Su, Y., Ng, T., Zhang, Y., Davidson, J.H., 2017. Three dimensional thermal diffusion in anisotropic heterogeneous structures simulated by a non-dimensional lattice Boltzmann method with a controllable structure generation scheme based on discrete Gaussian quadrature space and velocity. Int. J. Heat Mass Transf. 108, 386–401.
Tian, W., Fu, M.W., Qi, L., Chao, X., Liang, J., 2019. Interphase model for FE prediction of the effective thermal conductivity of the composites with imperfect interfaces. Int. J. Heat Mass Transf. 145, 118796.
Torquato, S., Rintoul, M.D., 1995. Effect of the Interface on the Properties of Composite Media. Phys. Rev. Lett. 75 (22), 4067–4070.
van Antwerpen, W., du Toit, C.G., Rousseau, P.G., 2010. A review of correlations to model the packing structure and effective thermal conductivity in packed beds of mono-sized spherical particles. Nucl. Eng. Des. 240 (7), 1803–1818.
Vieira, C.d.S., Marques, S.P.C., 2019. A new three-dimensional finite-volume model for evaluation of thermal conductivity of periodic multiphase composites. Int. J. Heat Mass Transf. 139, 412–424.
Wang, F., Li, X., 2017. The stagnant thermal conductivity of porous media predicted by the random walk theory. Int. J. Heat Mass Transf. 107, 520–533.
Wiener, O.H., 1912. Die theorie des Mischkörpers für das Feld der stationären Strömung. Abh. Math.-Phys. Kl. Königl. Sächs. Ges. 32, 509–604.
Xu, J., Gao, B., Du, H., Kang, F., 2016a. A statistical model for effective thermal conductivity of composite materials. Int. J. Therm. Sci. 104, 348–356.
Xu, J.Z., Gao, B.Z., Kang, F.Y., 2016b. A reconstruction of Maxwell model for effective thermal conductivity of composite materials. Appl. Therm. Eng. 102, 972–979.
Xu, P., Yu, B., Yun, M., Zou, M., 2006. Heat conduction in fractal tree-like branched networks. Int. J. Heat Mass Transf. 49 (19), 3746–3751.
Zhai, S., Zhang, P., Xian, Y., Zeng, J., Shi, B., 2018. Effective thermal conductivity of polymer composites: Theoretical models and simulation models. Int. J. Heat Mass Transf. 117, 358–374.
Zhang, H.F., Ge, X.S., Ye, H., Jiao, D.S., 2007. Heat conduction and heat storage characteristics of soils. Appl. Therm. Eng. 27 (2), 369–373.
Zhang, L.-Z., Wang, X.-J., Quan, Y.-Y., Pei, L.-X., 2013. Conjugate heat conduction in filled composite materials considering interactions between the filler and base materials. Int. J. Heat Mass Transf. 64, 735–742.
Zhao, W., Yang, Y., Bao, Z., Yan, D., Zhu, Z., 2020. Methods for measuring the effective thermal conductivity of metal hydride beds: A review. Int. J. Hydrogen Energy 45 (11), 6680–6700.
Zhou, F., Cheng, G., 2014. Lattice Boltzmann model for predicting effective thermal conductivity of composite with randomly distributed particles: Considering effect of interactions between particles and matrix. Comput. Mater. Sci 92, 157–165.